Title

Impaired Hippocampal-Cortical Interactions during Sleep in a Mouse Model of Alzheimer's Disease

Journal

Current Biology, 30(13)

ISSN

0960-9822

Authors

Benthem, Sarah D
Skelin, Ivan
Moseley, Shawn C
et al.

Publication Date

2020-07-01

DOI

10.1016/j.cub.2020.04.087

Peer reviewed

Published in final edited form as:

Curr Biol. 2020 July 06; 30(13): 2588–2601.e5. doi:10.1016/j.cub.2020.04.087.

Impaired Hippocampal-cortical interactions during sleep in a mouse model of Alzheimer's disease.

Sarah D. Benthem[1], **Ivan Skelin**[2,3], **Shawn C. Moseley**[1], **Alina C. Stimmell**[1], **Jessica R. Dixon**[1], **Aandreza S. Melilli**[1], **Leonardo Molina**[4], **Bruce L. McNaughton**[3,4], **Aaron A. Wilber**[1]

[1]Florida State Univ., Tallahassee, FL 32306

[2]Present Address: Dept. of Neurology, University of California Irvine, Irvine, CA 92697

[3]Dept. of Neurobiology and Behavior, University of California Irvine, Irvine, CA 92697

[4]Dept. of Neuroscience, University of Lethbridge, Lethbridge, Alberta, Canada T1K 3M4

Summary:

Spatial learning is impaired in humans with preclinical Alzheimer's disease (AD). We reported similar impairments in 3xTg-AD mice learning a *spatial reorientation task*. Memory reactivation during sleep is critical for learning related plasticity, and memory consolidation is correlated with hippocampal sharp wave ripple (SWR) density, cortical delta waves (DWs), cortical spindles, and the temporal coupling of these events - postulated as physiological substrates for memory consolidation. Further, hippocampal-cortical dyscoordination is prevalent in individuals with AD. Thus, we hypothesized impaired memory consolidation mechanisms in hippocampal-cortical networks could account for spatial memory deficits. We assessed sleep architecture, SWR/DW dynamics, and memory reactivation in a mouse model of tauopathy and amyloidosis implanted with a recording array targeting isocortex and hippocampus. Mice underwent daily recording sessions of rest-task-rest while learning the *spatial reorientation task*. We assessed memory reactivation by matching activity patterns from the approach to the unmarked reward zone to patterns during slow wave sleep (SWS). AD mice had more SWS, but reduced SWR density. The increased SWS compensated for reduced SWR density so there was no reduction in SWR number. In control mice, hippocampal SWR-cortical DW coupling was strengthened in *post-task*-sleep and was correlated with performance on the *spatial reorientation task* the following day. However, in AD mice SWR-DW and spindle-DW coupling were impaired. Thus, reduced SWR-DW coupling may cause impaired learning in AD and spindle-DW coupling during short rest-task-rest sessions may serve as a biomarker for early AD related changes in these brain dynamics.

Corresponding authors: Sarah Benthem and Aaron Wilber; benthem@psy.fsu.edu, awilber@fu.edu.
Lead Contact: Sarah Benthem

Author Contributions: Conceptualization, A.A.W.; Methodology, A.A.W., B.L.M., S.D.B., and S.C.M.; Formal Analysis, S.D.B., S.C.M., A.C.S., J.R.D., and A.S.M.; Software, S.D.B., I.S., and L.M.; Writing - Original Draft, S.D.B.; Writing - Review and Editing, A.A.W., S.D.B., and S.C.M.; Visualization, S.D.B.; Funding Acquisition, A.A.W. and B.L.M.

Declaration of Interest: The authors declare no competing financial interests.

Abstract

Benthem *et al.* use multi-site recordings to demonstrate increased sleep in AD mice that may compensate for some impaired brain dynamics. Cortical-hippocampal coupling during sleep predicts spatial learning in normal mice. However, spatial learning and cortical-hippocampal coupling are impaired in AD mice, possibly causing the impaired learning.

Introduction

Alzheimer's disease (AD) is devastating for both individuals and society [17]. Individuals with AD have memory, cognitive and navigational impairments; in fact, getting lost and having impaired orientation in space is an early hallmark of AD [18–20]. Rodent models of AD are characterized by similar spatial navigation impairments [21–24]. Spatial navigation and orientation involve hippocampal-parietal cortex (PC) interactions [25–42], and dysfunctional cortical-hippocampal interactions are a prominent feature in AD [43–50], including abnormal communication between the PC and hippocampus [43–46]. These findings, make the hippocampal-PC network an ideal model for studying altered hippocampal-cortical interactions in AD [47–51].

Memory consolidation involves cortical-hippocampal interactions, and changes in this network could be a contributing factor for AD-related memory impairments, particularly given evidence for altered cortical-hippocampal function in AD. The hippocampal formation is crucial to the storage of 'episodic' memories (memories for experiences that unfold in space and time), and for assisting the neocortex to extract generalized knowledge from these specific experiences [52]. It has been suggested that the hippocampus generates a unique code reflecting the spatiotemporal context of experience that links together components of a given experience by producing interactions between modules throughout the neocortex, including the PC [53, 54]. Hippocampus and PC exhibit coordinated replay during rest at both the single neuron [25, 55] and multi-neuronal (modular) level [25]. Memory reactivation has been proposed to be critical for neural changes underlying learning and memory [56–59]. In addition, mouse models of tauopathy and familial AD show changes in markers of memory replay. For example, the density and amplitude of hippocampal sharp wave ripples (SWRs) are reduced in these models [60–63]. Additionally, later in AD progression, both animal models and humans show changes in slow-wave sleep (SWS) [51, 64, 65]. Furthermore, impaired navigation-related learning and memory in AD mice is largely a consequence of forgetting from one day to the next [66]. Finally, AD involves synaptic changes that could impact memory formation [67, 68]. Thus, memory consolidation, which involves cortico-hippocampal interactions, is a potential mechanism for AD-related impairments. Specifically, pathological changes in the hippocampal-PC network may disrupt the functional hippocampal-PC interactions that enable sleep-related memory replay and therefore disrupt the binding of aspects of a given experience [69–71]. Here we examine hippocampal-PC brain dynamics during sleep following spatial learning behavioral sessions, to test the hypothesis that this system is disrupted in AD and may ultimately produce memory impairments in individuals with AD.

Results

Brain Dynamics During Sleep in Control Mice.

Female 3xTg-AD (APPSwe, PS1M146V, and tauP301L) mice (n=6) and age-matched NonTg mice (controls; n=6) from the same background strain underwent pretraining. The triple transgenic mouse model 3xTg-AD expresses three major genes associated with familial AD, as well as plaque and tangle pathology distributed similarly to that observed in humans [72]. Female 6-month 3xTg-AD mice have low levels of intracellular pathology (e.g., pTau and mOC78) and no extracellular plaques or tangles (e.g., ThioS) after several months of spatial learning [24]. After pretraining, a recording array targeting right PC and hippocampus (Figure S1A), and two bipolar electrodes targeting the medial forebrain bundle (mfb) were implanted. Then, training commenced on a spatial reorientation task [1, 24]. Daily recording sessions included a 50min sleep session, followed by 20min of task (real or virtual spatial reorientation task), followed by another 50min sleep session (Figure 1A). Mice completed more trials on the virtual maze (VM; 343% increase), therefore we focused on this data first. First, we tested the degree of temporal synchrony between the hippocampal and PC memory replay markers (SWRs and delta-waves) in NonTg mice during SWS (Figure 1B–C and Methods). Cortical replay tends to occur during the transitions between down- and up- states, and short down states correspond to the delta wave trough [DWT; 73]. Further, multiunit activity (MUA) template matching in PC is stronger during hippocampal SWRs, even after accounting for the influence of delta-waves [25]. Therefore, we assessed memory replay interactions across regions by cross-correlating DWTs with SWRs. We hypothesized that there would be a positive peak in the SWR-DWT cross-correlation. Since timing of the peak SWR-DWT correlation sometimes appears in slightly different time bins across animals and sessions (Figure S2), the peak value was compared irrespective of the precise time. NonTg mice had increased occurrence of SWRs immediately before DWTs (Figure 1D) in *post-task-sleep* (cream) versus *pre-task-sleep* (black). We measured the z-scored peak cross-correlation for *pre-task-sleep* compared to *post-task-sleep* in NonTg data sets that met inclusion criteria (see Methods). These recording sessions were divided into blocks of 3 days for the first 9 days of VM training and testing (n=28 data sets). Days 1–3 SWR-DWT coupling strengthened during *post-task-sleep*, though this was not statistically significant (Figure 1E; paired t-test: $t_{(8)}=-0.93$, p=0.38). Day 4–6 SWR-DWT coupling significantly strengthened during *post-task-sleep* ($t_{(6)}=-3.80$, p=0.004). However, day 7–9 coupling no longer increased in *post-task-sleep* and a negative relationship emerged. We also assessed the decreased SWR occurrence during the DWT by assessing the negative peak, and found no significant difference for any period (days 1–3 & 7–9: $ts_{(1,\ 9–10)}<1.86$, ps>0.09; days 4–6: $t_{(1,6)}=-2.48$, p=0.04, ns with Bonferroni correction; critical p=0.017).

Next, we looked for evidence of memory replay in the PC of NonTg mice using template matching, a method we previously used for detecting memory reactivation in rat PC [25]. Note, we operationally define memory reactivation or replay as matching activity patterns from a *task* to *post-task-sleep* and acknowledge that we are not directly measuring ‘memory’ per se. Cortical memory replay is temporally compressed [Figure 2; 25, 74], so we compared non-compressed and compressed templates across a range of compression factors [‘non-compressed’, 4x, 6x, 8x, and 10x; as in our previous paper 25]. We found template matching

was strongest with 6x compression (i.e., activity sequences are reactivated 6x faster than during behavior; Figure 2A–C), consistent with previous findings of temporally compressed memory replay [25, 73–76]. Finally, we assessed potential influences of time or training phase on memory reactivation. We focused on days 1–9 of the VM task, the same time course as the SWR-DWT analyses (n=20 data sets; Table S1). During VM days 1–3 and 4–6, most data sets (81% and 86%) showed an increase in strong template matches in *post-task-sleep* (Figure 2D). However, day 7–9 *post-task-sleep* template matching increased in only 50% of the data sets. Thus, PC memory replay is strong during the first 6 days of training, then falls off.

Impaired Spatial Learning and Memory.

Next, we looked for impaired virtual spatial reorientation performance to see if similar deficits occur on the VM as our published data from the real maze [n=5 mice/genotype; 24]. On the VM, mice are teleported to a random start location and use distant cues to orient to the maze space and locate an unmarked reward zone (Figure 2A), where they pause for a period to obtain a reward, with increasing delays (see Methods). First, we compared z-scored velocity in the reward zone with velocity immediately prior to the reward zone for NonTg mice. NonTg mice slowed in the reward zone in days 1–3, as well as days 4–6 of the VM task (Figure 3 *Top*; paired t-test; n=5/group, $ts_{(1,14)} \geq 2.11$, $ps \leq 0.05$). When we performed the same analysis for days 7–9, NonTg mice continued to slow despite the increasing difficulty as reward delays increased ($t_{(1,14)}=2.97$, $p=0.01$). We hypothesized that NonTg mice should more effectively orient themselves using distal cues and slow more in the reward zone than 3xTg-AD mice, which is what we found (Figure 3 *Bottom;* two-way RMANOVA; $F_{(1,7)}=9.00$, $p=0.01$, no day main effect or day-by-genotype interaction; $Fs_{(5,35)} \leq 1.13$, $ps \geq 0.36$). Thus, NonTg mice were better at learning to use distant maze cues to locate the virtual goal zone. We performed the same assessment on days 7–9 of the VM task and found that 3xTg-AD mice no longer performed worse than NonTg mice ($F_{(1,7)}=2.27$, $p=0.17$). Given that both template matching in PC and coupling with hippocampus dropped dramatically after VM day 6, and that 3xTg-AD mice were not impaired after 6 days, we limited our assessment of memory reactivation to the first 6 VM days.

At 6-months 3xTg-AD mice have better motor ability than controls, though impairments emerge later [77, 78]. So, we assessed the mean velocity from a portion of the track before mice begin slowing for the reward zone to ensure differences in running speed were not contributing to the observed effects. As for the real-world version of this task [24], there was no difference in movement velocity across genotype (two-way RMANOVA; $F_{(2,7)}=2.66$, $p=0.14$, no day effect or interaction, $Fs_{(2,10)} \leq 1.07$, $ps \geq 0.41$).

Compensatory Sleep Changes.

Effects on sleep quality have been reported in AD [79]; however, those reports focused on later stages of disease progression (e.g., post-plaque formation). The 6-month 3xTg-AD female mice examined here have intracellular phosphorylated Tau and Aβ [24] but no extracellular tangles or plaques, so sleep quality in 3xTg-AD mice at this stage was unknown (e.g., time still, proportion still time in SWS). As described above, we limited

analyses to VM days 1–6 (18 NonTg and 14 3xTg-AD data sets). Surprisingly, we found that NonTg mice were motionless less than 3xTg-AD mice (Figure 4 *Top Left*; n=5 NonTg, n=6 3xTg-AD; two-way RMANOVA; $F_{(1,31)}$=7.493, p=0.01) but no *pre-task-sleep* versus *post-task-sleep* phase or genotype by sleep-phase interaction ($Fs_{(1,31)}$≤0.91, ps≥0.34). NonTg mice also had shorter average uninterrupted SWS episodes ($F_{(1,30)}$=7.51, p=0.003), but no sleep-phase effect or interaction ($Fs_{(1,30)}$≤1.69, ps≥0.20). Interruptions to SWS could be caused by entering rapid eye movement (REM) sleep or waking, so we assessed REM. We found that REM sleep proportion decreased during *post-task-sleep* ($F_{(1,30)}$=6.64, p=0.01) regardless of genotype (Figure S3; also no genotype-by-sleep-phase interaction $Fs_{(1,30)}$ ≤1.62, ps≥0.21). However, number REM episodes remained constant ($F_{(1,30)}$=2.46, p=0.12, no genotype effect or interaction; $Fs_{(1,30)}$≤0.21, ps≥0.54). The decrease in REM corresponded to increased SWS from *pre-task-sleep* to *post-task-sleep* ($F_{(1,30)}$=13.02, p=0.001) regardless of genotype (also no interaction; $Fs_{(1,30)}$≤0.57, ps≥0.45). Thus, SWS increased after the task regardless of genotype and NonTg mice slept less than 3xTg-AD mice.

Next, we performed the same analysis using animal means and again stillness did not vary across genotype (Figure S4; no sleep-phase effect or interaction; $Fs_{(1,9)}$ ≤2.31, ps≥0.16). SWS again did not vary across genotype (also no sleep-phase or genotype-by-sleep-phase interaction; $Fs_{(1,8)}$ ≤3.74, ps≥0.08). However, 3xTg-AD mice had increased SWS episode length ($F_{(1,8)}$=16.13, p=0.003, no sleep-phase effect or genotype-by-sleep-phase interaction $Fs_{(1,8)}$ ≤0.71, ps≥0.42). Unlike when data sets were used as the n, REM proportion did not vary across sleep-phase ($F_{(1,8)}$=1.22, p=0.29, no genotype effect or genotype-by-sleep-phase interaction $Fs_{(1,8)}$ ≤0.99, ps≥0.34). Thus, when animals were used as the n key results were unchanged.

Next, we assessed memory reactivation markers, PC DWTs and sleep spindles, and hippocampal SWRs. Since 3xTg-AD mice were still more and had increased SWS episodes versus NonTg mice, we assessed both density (Figure 4 *Top Right*) and number (Figure 4 *Bottom Left*) of events. SWR density decreased in 3xTg-AD mice versus NonTg mice ($F_{(1,30)}$=9.68, p=0.004; no genotype effect or genotype-by-sleep-phase interaction, $Fs_{(1,30)}$ ≤0.81, ps≥0.37). However, the total number of events was not different across genotype or sleep-phase and there was no interaction ($Fs_{(1,30)}$≤1.05, ps≥0.31). Consistent with the known correlation between SWRs and spindles [80], spindle density was decreased in 3xTg-AD mice ($F_{(1,29)}$=4.71, p=0.03, no sleep-phase effect or interaction; $Fs_{(1,29)}$≤0.12, ps≥0.72). However, the number of spindles did not vary across genotype ($F_{(1,29)}$=3.26, p=0.08, no sleep-phase effect or interaction; $Fs_{(1,29)}$≤0.86, ps≥0.36). The density of DWTs was equivalent across genotype (also no genotype effect or interaction; $Fs_{(1,30)}$≤0.32, ps≥0.57). In addition, the total number of DWTs was not significantly different across genotype ($F_{(1,31)}$=3.66, p=0.06). However, the total number of DWTs was increased in *post-task-sleep*, consistent with the increase in SWS ($F_{(1,31)}$ = 127.33, p≤0.0001; no interaction; $F_{(1,31)}$=0.27, p=0.26).

Next, we assessed markers of memory reactivation with animals as n (Figure S4). The density of SWR was reduced in 3xTg-AD mice ($F_{(1,8)}$=7.46. p=0.02, no sleep-phase effect or interaction $Fs_{(1,8)}$ ≤0.06, ps≥0.80). Again, SWR number did not vary across genotype

(also no sleep-phase effect or interaction; $Fs_{(1,8)} \leq 1.03$, $ps \geq 0.33$). However, with animals as n, the spindle density was no longer reduced as when data sets were n (also no sleep-phase effect or interaction; $Fs_{(1,8)} \leq 1.32$, $ps \geq 0.28$). Spindle number did not vary across genotype (also no sleep-phase effect or interaction; $Fs_{(1,8)} \leq 1.79$, $ps \geq 0.22$). DWT density also did not vary across genotype (also no sleep-phase effect or interaction; $Fs_{(1,8)} \leq 1.16$, $ps \geq 0.41$). Similarly, DWT number did not vary across genotype (also no sleep-phase effect or interaction; $Fs_{(1,9)} \leq 0.84$, $ps \geq 0.38$). Thus, with the exception of spindle density, identical results were obtained with animals used as the n.

Next, we assessed the relationship between density and number of SWRs, spindles, and DWTs during *post-task-sleep* and behavioral performance the following day. Total number and density of SWRs and spindles were not significant predictors of performance for either genotype ($rs \leq 0.38$, $ps \geq 0.22$). DWT number also did not predict performance the subsequent day for either group ($rs \leq 0.47$, $ps \geq 0.14$). However, DWT density did predict performance the following day for NonTg (Figure 4, *Bottom left;* $r=-0.48$, $p=0.02$) but not 3xTg-AD (Figure 4, *Bottom right;* $r=0.30$, $p=0.25$) mice. The correlation was significantly stronger for NonTg than 3xTg-AD mice (Fisher r-to-z transformation; $z=-2.1$, $p=0.03$). Thus, *post-task-sleep* DWT was a significant predictor of behavior on the virtual maze for NonTg animals only.

Impaired Hippocampal-PC Interactions.

Next, we assessed hippocampal-PC interactions to see if 3xTg-AD mice had changes in network dynamics that could reflect impaired cross-structure coordination of memory replay (n=14 3xTg-AD data sets met the inclusion criteria). We assessed hippocampal-PC coupling by cross-correlating PC DWTs with hippocampal SWRs, as described above. We assessed the proportion of data sets with a larger *post-task-sleep* verses *pre-task-sleep* peak in the SWR-DWT correlation. In NonTg mice, a significantly larger proportion of data sets (78%; Figure 5 *Top Left*) showed an increase in SWR-DWT correlation, versus 3xTg-AD mice (36%; Figure 5 *Top Right*, $\chi^2_{(1)}=5.77$, $p=0.01$), suggesting that hippocampal-cortical coordination of memory replay events was impaired in 3xTg-AD mice. Next, we assessed the relative timing of these two events. For SWS periods, NonTg mice had increased occurrence of SWRs immediately before DWTs (Figure 5 *Middle Left*) in *post-task-sleep* versus *pre-task-sleep* ($t_{(17)}=2.25$, $p=0.003$). However, for 3xTg-AD mice, the SWR-DWT relationship was smaller, and not significantly increased in *post-task-sleep* (Figure 5 *Middle Right*, paired t-test; $t_{(13)}=1.21$, $p=0.25$). We also assessed the decrease in SWR near the DWT by assessing the negative peak (minimum value). There was a reduction in NonTg mice ($t_{(17)}=-2.78$, $p=0.01$) that was not predictive of performance ($r=0.08$, $p=0.75$), and 3xTg-AD mice showed no change ($t_{(13)}=-0.77$, $p=0.46$). Thus, hippocampal-cortical coupling is impaired in 3xTg-AD mice.

We also assessed hippocampal-cortical coupling using animals as the n. In NonTg mice SWR-DWT coupling increased in *post-task-sleep* relative to *pre-task-sleep* (Figure S5, $t_{(4)}=3.69$, $p=0.02$). However, in 3xTg-AD mice the pattern reversed and there was a decrease in coupling in *post-task-sleep* (Figure S5, $t_{(4)}=-2.80$, $p=0.04$). Thus, equivalent results are obtained whether data sets or animals are used as the n.

Finally, we assessed the relationship between SWR-DWT correlations and VM performance. We calculated a z-scored peak ratio by dividing the z-scored peak from *post-task-sleep* by the z-scored peak from *pre-task-sleep* and compared this to performance on the VM the subsequent day. This ratio predicted performance in NonTg (Figure 5 *Bottom Left*, r=−0.49, p=0.03), but not 3xTg-AD (Figure 5 *Bottom Right*, r=0.24, p=0.47) mice. NonTg mice had a stronger correlation than 3xTg-AD mice (Fisher r-to-z transformation, z=−1.97, p=0.04). As an additional control, we assessed the relationship between this ratio and performance the same day. Neither genotype showed a relationship between the z-scored peak ratio of SWR-DWT correlations and same day performance (rs≤0.49, ps≥0.10). This suggests that SWR-DWT correlations may represent plasticity that produces better performance the following day and this coupling is absent in 3xTg-AD mice.

Next, we performed the same analysis on the first six days of the real-world task to see if we could detect similar deficits despite fewer trials. Once again, NonTg mice showed a greater proportion of data sets with an increase in SWR-DWT coupling in *post-task-sleep* compared to 3xTg-AD mice, though the difference was not statistically significant (80% for NonTg, 42% for 3xTg-AD; Figure S5; $\chi^2_{(1)}$=3.32, p=0.06). Thus, the larger number of trials in the virtual maze may be critical for detecting altered brain dynamics during sleep in 3xTg-AD mice.

In order to assess that the increase in SWR-DWT correlations represented hippocampal dependent learning, we assessed whether there was a similar increase during operant training to nose poke for mfb stimulation (see methods). We found task-induced increases in SWR-DWT coupling in 63% of data sets for NonTg mice, which did not significantly differ from 3xTg-AD mice (40%; Figure S5; $\chi^2_{(1)}$=0.63, p=0.43), suggesting the effects we observed are specific to tasks which preferentially engage a hippocampal-cortical network.

Impaired Spindle-DWT Coupling.

Some have suggested that SWRs, delta waves, and spindles are all temporally correlated in order to facilitate memory consolidation [81], so we assessed these relationships. First, we assessed temporal correlations between hippocampal SWRs and cortical spindles and consistent with previous reports [80–83] found that for both genotypes there was a strong temporal correlation between the SWR peak and spindle onset (Figure S6). Next, given that spindles tended to occur after the DWT in NonTg mice (e.g., Figure 6 *Top Left*), we looked to see if cortical spindles might be a good proxy for hippocampal SWRs. We assessed spindle-SWR correlations, using the same approach used for DWT-SWR correlations. We assessed the proportion of data sets with a larger *post-task-sleep* verses *pre-task-sleep* peak in the spindle-SWR temporal correlation. We found task-induced increases in spindle-SWR coupling in 70% of NonTg data sets, similar to SWR-DWT correlations, but the proportions were not significantly lower in 3xTg-AD mice (57% of data sets; Figure 6 *Top Right;* $\chi^2_{(1)}$=0.61, p=0.44). We hypothesized that this approach might not be sensitive enough to detect spindle-DWT coupling, given the longer duration of spindles. We also employed a measure used for analyzing sleep EEG recordings in humans. We compared the DW phase and the peak in spindle power [81, 84]. For NonTg mice, peak spindle power tended to occur at the peak of the delta wave (Figure 6 *Bottom Left*) but was distributed across phases in

3xTgAD mice (Figure 6 *Bottom Right*). As a result, the phase distributions differed significantly ($F_{(1,60)}$=13.3, p<0.001). Thus, spindle-DWT coupling is impaired in 3xTg-AD mice.

Aβ Relationship with Brain Dynamics During Sleep.

Next, we assessed correlations between pathology and behavioral deficits. At 6-months of age Aβ aggregation is apparent intracellularly, but extracellular Tau and Aβ aggregation is not yet apparent [24, 85]. Therefore, we quantified the z-scored density of neurons with intracellular β-Amyloid 1–16 staining (6e10, Figure S1B) in ventral CA1 of the hippocampus, dorsal CA1, and PC. We found no significant relationships between z-scored velocity in the reward zone (spatial memory) and $6e10^+$ cell density for any region (Table S2; $|rs| \leq 0.66$, ps≥0.23). Next, we assessed the relationship between $6e10^+$ cell density and SWRs, DWTs, and spindles. SWR number was negatively associated with $6e10^+$ cell density in ventral and dorsal CA1 ($|rs| \geq 0.88$, ps≤0.04), but not PC (r=−0.65, p=0.23). Surprisingly, DWT number and rate were also significantly negatively associated with $6e10^+$ cell density in dorsal ($|rs| \geq 0.86$, ps≤0.03), but not ventral CA1 or PC ($|rs| \leq 0.83$, ps≥0.07). Spindle rate was significantly negatively associated with $6e10^+$ cell density in in ventral and dorsal CA1 ($|rs| \geq 0.96$, ps≤=0.01), but not PC (r=−0.62, p=0.26). Spindle number was negatively associated with $6e10^+$ cell density in dorsal CA1 (r=−0.95, p=0.01), but not ventral CA1 or PC ($|rs| \leq 0.78$, ps≥0.12). Next, we assessed the relationship between $6e10^+$ cell density and SWR-DWT and SWR-spindle correlations. Z-scored peak of SWR-DWT post/pre ratio was not associated with $6e10^+$ cell density in any region analyzed ($|rs| \leq 0.79$, ps≥0.11). Similarly, SWR-spindle correlations were not associated with $6e10^+$ cell density in any region analyzed ($|rs| \leq 0.61$, ps≥0.28). CA1 $6e10^+$ cell density being significantly correlated with both hippocampal and cortical events while cortical $6e10^+$ cell density was not suggests that hippocampal pathology may provide the best index of brain dysfunction during sleep, even for brain regions several synapses away.

Intact PC Reactivation.

Finally, we assessed reactivation of activity patterns within PC. In NonTg mice, memory replay was compressed by 6x (Figure 2C). We also assessed template matches in 3xTg-AD mice at a range of compression factors (n=9 3xTg-AD data sets from 3 animals met the inclusion criteria, see Table S1). Note, the lower number of 3xTg-AD data sets was due to fewer data sets with ≥6 tetrodes in PC (Table S1). For 3xTg-AD mice, template matches oscillated around 40% for all compression factors with peaks at 6x and 10x (Figure 7 *Left*). First, we used 6x compression, since this was ideal for NonTg mice. We compared the proportion of strong template matches between *pre-task-sleep* and *post-task-sleep* across genotype. NonTg mice had more strong template matches in *post-task-sleep* (81%) compared to 3xTg-AD mice (67%), but this difference was not statistically significant (Figure 7 *Middle*; $\chi^2_{(1)}$=0.67, p=0.41). Since 3xTg-AD mice had equivalent template matching with 6x or 10x compression applied, we performed the same comparison with 10x compression. There was again no significant difference between the two groups (62% for NonTg and 78% for 3xTg-AD mice; $\chi^2_{(1)}$=0.62, p=0.43) and there was no significant improvement in template matching in 3xTg-AD mice with10x versus 6x compression ($\chi^2_{(1)}$=0.22, p=0.64). In addition, to ensure that 3xTg-AD animals were not showing a

change in the ideal compression factor, we compared data from NonTg mice with 6x compression to 3xTg-AD mice with 10x compression. Again, there was no significant difference, suggesting that a shift in the rate of replay does not explain the lower proportion observed in 3xTg-AD mice (81% for NonTg and 78% for 3xTg-AD mice; $\chi^2_{(1)}$=0.04, p=0.83).

Next, we assessed the strength of 6x compressed template matching (Mean±SEM) centered on the DWT. Template matches were z-scored and averaged for *pre-task-sleep* and *post-task-sleep* for both genotypes. Both genotypes exhibited a decrease in matches during the DWT, followed by an increase in matches during the upstate transition, with no difference across genotype (Figure 7 *Right*). Thus, the temporal relationship between template matches and DWTs remained consistent between both sleep sessions for both groups.

Finally, to examine the possibility that reverse replay [76, 86] might be altered in 3xTg-AD mice, we assessed reverse template matching. We found that for NonTg and 3xTg-AD mice, 8x compression produced the highest reverse template matching. Next, we compared the proportion of data sets with higher *post-task-sleep* template matching and found there was no difference between genotypes (88% for NonTg and 67% for 3xTg-AD mice; Figure S7; $\chi^2_{(1)}$=1.56, p=0.21).

Discussion

We assessed memory replay as a potential mechanism for spatial reorientation learning deficits we reported previously [24]. We found that 3xTg-AD mice have increased time spent in sleep, but reduced SWR density. However, the longer duration of SWS meant that the number of SWRs was not reduced. Finally, we found that in NonTg mice, hippocampal SWRs occurred in close temporal proximity to PC DWs. This coupling was strengthened in *post-task-sleep* and correlated with performance on the *spatial reorientation task* the following day. However, in AD mice, SWR-DW coupling was reduced and uncorrelated with behavioral performance. This suggests a dissociation between memory replay events for 3xTg-AD mice and subsequent behavioral performance, i.e., the expected benefit from memory reactivation between behavioral training and testing is not occurring. In addition, DWT rate was significantly correlated with behavior in NonTg mice, but not 3xTg-AD mice, suggesting that DWTs become dissociated from behavior without the SWR coupling. Finally, cortical spindles were highly correlated with SWRs for NonTg and 3xTg-AD mice, and spindle phase locking to DWTs was impaired in 3xTg-AD mice. These findings suggest that assessing task-induced brain dynamics in humans with EEG (spindle-DWT coupling) may be a useful biomarker of very early changes in AD.

We observed a potential compensatory sleep pattern in 3xTg-AD mice early in disease progression (i.e., intracellular Tau and Aβ, no plaques or tangles). 3xTg-AD mice had increased time in SWS, leading to preserved number of SWRs despite a reduction in density. This suggests the possibility that increased time in SWS is an early compensatory mechanism for changes in sleep physiology in 3xTg-AD mice. Similar compensatory changes have not been reported in humans, though sleep disturbances are associated with mild cognitive impairment and with AD [84, 87–99]. In humans, sleep changes, include

diminished quality (increased fragmentation, increased time to sleep onset but retention of total sleep time), that emerge in parallel with initial Aβ increase in the cerebrospinal fluid [91, 100–102]. In addition, disruption of sleep increases levels of CSF Aβ in both cognitively normal adults and AD patients [103–105]. It has been theorized that SWS clears Aβ from the brain into CSF [106]. Most studies find that sleep disruption and SWS sleep deficits are associated with increased Aβ, assayed with PET imaging [107–109]. However, one study that measured brain Aβ with PET and CSF Aβ, found that CSF Aβ is negatively correlated with brain Aβ, suggesting Aβ is trapped in the brain and not cleared into the CSF [110]. Furthermore, lack of sleep, as well as increased sleep disturbances have been associated with increased risk of AD, amyloid deposition, and cognitive impairment [84, 92, 94, 100, 111, 112] and conversely there is evidence that SWS increases Aβ clearance [64, 113]. If SWS clears Aβ, the increased sleep time we see prior to Aβ plaque formation may be a compensatory mechanism to dampen early pathological processes.

Like humans, animal models display sleep abnormalities concurrent with Aβ deposition [114–120]. Some mouse models show decreases in sleep after Aβ plaques begin forming [65, 79, 115], consistent with the possibility that the increased sleep we observed may be an early compensatory mechanism that eventually breaks down as pathology progresses. However, an amyloidosis only mouse model (APP/PSEN) had decreased time spent in sleep prior to the development of plaques [116], and time after the development of Aβ plaques the Tg2576 model does not have deficits in sleep [119]. A possible explanation for this is that the effects of Aβ or Tau alone might produce a different pattern of sleep changes than both Tau and Aβ together as occurs in 3xTg-AD mice. However, 3xTg-AD mice at 8–10 months, show no changes in total sleep time or NREM and SWS proportions [121], indicating that our finding is potentially an activity induced increase (i.e., is only apparent when short periods of sleep surrounding a task are assessed), or perhaps rapidly dissipates. Late tangle pathology alone also influences sleep as post-tangle formation $PLB2_{Tau}$ mice have reduced total sleep time and NREM sleep [122]. Together, this past and present data suggest that the influence of tau and Aβ on sleep is complex, may vary over the course of disease progression, and may produce a different phenotype than either pathology component alone.

Abnormally rigid sequences of cell activity have been reported in AD mice in the mature stages of disease progression, as mouse models of Tauopathy and familial AD have shown changes in characteristics of hippocampal SWRs, after neurodegeneration [62, 63, 123]. These changes include decreased density of SWRs, consistent with our results [60, 63]. However, these reports did not assess the influence of sleep on SWR number. Our findings suggest that deficits in density of SWR generation may appear early in AD, but initially, sleep changes may prevent a reduction in the SWR number.

Replay of activity patterns during sleep is critical for learning and memory, including navigation [56, 59]. The hippocampal formation is thought to be crucial to the storage of ‘episodic’ memories, and assists the neocortex extract generalized knowledge from these experiences [52]. Because the hippocampus is critical for recent memories, it has been suggested that it generates a unique code reflecting the spatial-temporal context of experience [124–127]. This code has been suggested to provide a ‘trace’ or ‘index’ that links together components of a given experience that are independently stored in weakly

interacting modules throughout the neocortex, including the PC [53, 54]. The hippocampal output at the time of experience has been theorized to enable indirect, coordinated retrieval of episodic information from these modules. For recent memories, the hippocampus appears to orchestrate retrieval of information throughout cortex [82]. The process may be initiated in the neocortex for older memories [127–129]; however, more recent theories and data suggest that hippocampal involvement may remain much longer than originally theorized [127, 129]. We found that in 3xTg-AD mice that have not yet presented with tangles and plaques, there is a robust deficit in hippocampal-PC interactions during sleep, while memory replay events in PC are not significantly altered. Thus, the learning and memory deficits we observed may represent a failure of memory indexing or trace formation as a result of altered cortical-hippocampal interactions.

Spindle coupling with slow delta phases differs between young and old adults [81, 84]. Similarly, the distributions of slow delta phase coinciding with spindle peaks were significantly different between the 3xTg-AD and NonTg mice. In addition, spindle-DW coupling phases in 3xTg-AD mice were widely distributed, possibly reflecting a suboptimal spindle-delta coordination, suggested to be important for hippocampal-dependent memory consolidation [80, 81, 130–134]. This suggests a parallel pattern of results in rodents and humans that can be extended into the realm of understanding the relationship with SWRs in rodents.

Extracellular amyloid β deposition and Tau tangles were absent in the 3xTg-AD mice in the present paper. In addition, other studies have also found no gross changes in synaptic structure in the 3xTg-AD mouse model until a later time point, 9 months [135]. However, the proportion of cells positive for intracellular Aβ was correlated with DWTs, SWRs, and spindles, suggesting there are functional changes associated with Aβ at this early timepoint. Consistent with this finding, functional changes in synaptic communication emerge just prior to the timepoint assessed here, including Long Term Potentiation (LTP) deficits apparent in 3 and 6-month 3xTg-AD mice [135, 136]. Thus, it is possible that very early changes in synaptic function account for the impaired hippocampal-cortical coupling. Such a parallel is consistent with the theoretical role of brain dynamics in creating an environment for LTP-like mechanisms of memory consolidation [124, 137, 138]. Furthermore, the deficits we observed could also lead to retrieval issues related to dysfunctional LTP-like memory mechanisms in memory replay failing to adequately strengthen retrieval pathways [139].

In the 3xTg-AD mouse model, we see sleep changes early in disease progression, with increased sleep time compensating for decreased SWR density. However, these changes fail to compensate for all dysfunction. Impairments remain in hippocampal-PC interactions, with deficits in experience induced increases in SWR by DWT coupling. Furthermore, these hippocampal-PC deficits correlate with VM impairments. Thus, AD may cause hippocampal-cortical network changes which impair spatial orientation because of impaired learning related plasticity particularly between PC and hippocampus during SWS.

STAR Methods

Resource Availability

Lead Contact—Further information and requests for resources and reagents should be directed to the Lead Contact, Sarah Benthem (sdb18f@fsu.edu).

Materials Availability—This study did not generate any unique reagents.

Data and Code Availability—Further information and requests for the data sets and code generated by this study should be directed to and will be fulfilled by the Lead Contact, Sarah Benthem (sdb18f@fsu.edu).

Experimental model and subject details—Female 3xTg-AD (APPSwe, PS1M146V, and tauP301L) mice (n=6) and age-matched NonTg mice (controls; n=6) from the same background strain were group housed (2–4/cage) in 12:12 hour light-dark cycles until the experiment began. The triple transgenic mouse model, 3xTg-AD, expresses three major genes associated with familial AD, as well as plaque and tangle pathology with a distribution pattern comparable to that observed in humans [72]. Controls were bred by crossing 129x mice with C57BL/6 mice. Animals were originally obtained from Dr. Frank LaFerla (University of California, Irvine) and bred in our vivarium. Mice were 6–7 months at the beginning of the experiment. All experimental procedures were carried out in accordance with the NIH Guide for the Care and Use of Laboratory Animals and approved by the University of California, Irvine (n=1 mouse) and Florida State University Animal Care and Use Committee (n=11 mice).

METHOD DETAILS

Behavior

Pretraining.: Mice were moved to single housing and water deprived to no less than 80% of their starting weight. Then *alternation training* began where mice learned to shuttle back and forth along a linear track for a water reward that was delivered in the start-box only (i.e., rewarded for each traversal out to the end of the track and back to the start box). At the end of the track was a black barrier in front (from the mouse's perspective) of a black background. The starting position was moved to different locations by sliding the entire track, while the barrier remained fixed, resulting in variation in track length. Starting positions were randomly selected, between 56–76cm from reward zone. When mice met asymptote criteria (number of runs did not vary by more than ±6 on 3 of 4 days, or ran 50 or more times down the track in a single session), a date was scheduled for implantation of stimulating electrodes and the recording array. Mice continued to run the task every other day leading up to implantation surgery, including the day before surgery.

Surgical Procedure.: *Two bipolar* stimulating electrodes were implanted unilaterally, targeting the left mfb (1.9mm & 1.4mm posterior to bregma, ±0.8mm lateral, 4.8mm below dura). A 16-tetrode recording array [140] was implanted, targeting the right PC and dorsal hippocampus (2.2mm posterior to bregma, 2.0mm lateral). Animals recovered for one week, during which tetrodes targeting PC were moved down 31μm daily for the first three days,

and then every other day, to prevent sticking. Tetrodes were not advanced beyond the lower border of PC, as determined based on inspection of the LFP, and depth records. Tetrodes targeting hippocampus were turned down up to 124μm daily for the first three days, and then 31μm every other day, until tetrodes reached hippocampus, as indicated by depth records, as well as the characteristic hippocampal LFP. Tetrode locations were histologically verified *post-mortem*, based on the presence of electrolytic lesion corresponding to the tetrode tip (Figure S1A).

Stimulation parameters.: After recovery, animals were placed in a custom 44 × 44 × 44cm black box with a nose poke port (Med Associates) in the left corner. Electrical stimulation lasting 500ms was administered manually to shape the mice to use the nose poke port. Nose pokes were registered by a custom MATLAB program that automatically delivered stimulation. Once mice had been trained to use the nose poke port, stimulation parameters were varied (171–201Hz, 30–130μA current, electrode wire combination) to identify the settings that produced the highest response. No attempt was made to balance settings across genotype. However, response rate was compared across genotype to ensure that differences in reward strength were not likely to contribute to observed effects, and did not vary across genotype ($t_{(10)}$=0.69, p=0.50). The same comparison was made for the two brain stimulation parameters that were adjusted, frequency ($t_{(10)}$=0.15, p=0.88) and current ($t_{(10)}$=0.15, p=0.88), which also did not vary across genotype.

Spatial Reorientation Training.: After optimal stimulation settings were identified, mice completed a spatial reorientation task previously described [1, 24]. Briefly, the *spatial orientation task* is identical to *alternation training*, except for the addition of an 8cm long goal zone in a fixed location in the room. For this task, if the mouse pauses in the real or virtual (for the virtual maze version described below) goal zone for a sufficient period, brain stimulation reward is delivered. The required duration of the pause in the goal zone gradually increases as the animal achieves asymptote criterion at each phase (0.5–2.5s in 0.5s increments). The real (or virtual) box and track are moved after each trial (sliding track or virtual teleportation), so the goal zone remains at a constant position within the real (or virtual) room; however, the goal zone can be at a variety of distances from the start box (40–110cm). The velocity profile during the approach to the reward zone (slowing) is used to assess performance [1, 24]. Asymptote criteria was ±15% correct trials over 3 out of 4 consecutive days. Most data reported here comes from the next (virtual) task for which mice run many more trials per daily recording session (343% increase).

Virtual Maze.: Upon completion of the spatial reorientation task, mice were trained on a VM [https://www.interphaser.com/, 141] as described above. The only difference was the addition of an acclimation period for learning to navigate the VM during head fixation. Note, prior to this point mice are head fixed daily for approximately 1-month while turning tetrodes, so acclimation to head fixation has already occurred. The acclimation period during VM training is to allow the animal to learn how to control the VM environment while head fixed. Most mice prefer a specific head orientation for navigating the VM and it takes some time to find the optimal head orientation for each mouse. Head fixation was performed by clamping the head fixation device into place for most mice (67%), except for a subset of

mice that preferred the freedom to assume a slightly larger range of head orientations while navigating the VM (2 mice from each genotype; 33%). For these mice that preferred a more flexible head orientation while navigating the VM this flexibility was most easily attained with hand fixation. Note, hand fixation means that the head clamp was held manually instead of locking it into place. The actual mouse was not touched during hand fixation. In addition, 1 mouse was unable to tolerate even the hand fixation, and this data was excluded from VM analyses. The tablet was coated with a thin layer of mineral oil and the mouse was allowed to run on the tablet in place (note, tetrode turning takes place on a mineral oil coated tablet that is not powered on thus habituating the mouse to head fixation). The mouse's paws were sensed on the floor tablet similar to a finger swipe on a cell phone screen, which caused the virtual environment to move at the same rate as if the mouse was running across a real floor. Virtual movement was restricted to forward or backward only (the virtual environment could not turn). Three wall tablets (front and both sides) were synced to the floor tablet to display the view of the virtual room.

Recording Procedures.: An electrode interface board (EIB-72-QC-Small or EIB-36–16TT Neuralynx) was attached with a custom adapter to the recording array [140] with independently drivable tetrodes connected via a pair of unity-gain headstages (HS-36 Neuralynx) to the recording system (Digital Lynx SX Neuralynx). Tetrodes were referenced to a tetrode wire in the corpus callosum and advanced as needed, up to 62μm/day, while monitoring the audio and visual signal of the unit activity. Each daily recording session included a 50min sleep session, followed by 20min of task (real or virtual maze), followed by another 50min sleep session (Figure 1A). Adjustments were made after a given day's recording to allow stabilization overnight. Thresholded (adjusted prior to each session) spike waveforms were bandpass-filtered 0.6–6kHz and digitized at 32kHz. A continuous trace was simultaneously collected for processing as LFP from one of the tetrode wires (bandpass-filtered 0.1–1000Hz and digitized at 6400Hz) and referenced to an electrode in corpus callosum. Mouse position was tracked using a colored dome of reflective tape for the real maze (or virtual position for the virtual maze), and on-line position information was used to trigger mfb stimulation rewards. Video-tracking or virtual position data was collected at 30Hz and co-registered with spikes, LFPs, and event timestamps.

Spike data were automatically overclustered using KlustaKwik and manually adjusted using a modified version of MClust (A.D. Redish). All spike waveforms with a shape, and across tetrode cluster signature suggesting that they were likely MUA and not noise, were manually selected and merged into a single MUA cluster. Thus, MUA clusters included both well-isolated single units and poorly isolated single units [http://klustakwik.sourceforge.net; 142].

LFP analyses were performed using custom-written Matlab code (Mathworks, Nattick, MA) or Freely Moving Animal (FMA) Toolbox (http://fmatoolbox.sourceforge.net/). The LFP signal was collected at 6400Hz and subsequently resampled to 2000Hz for further analysis, using the Matlab *resample* function.

Histology.: At the conclusion of the experiment, marking lesions were made by applying a 5μA current for 10s between each tetrode wire and the tail. One week later mice were given an intraperitoneal injection of Euthasol and then transcardially perfused with 0.1M

phosphate-buffered saline (PBS), followed by 4% paraformaldehyde (PFA) in 0.1M PBS. The whole head was post-fixed for 24h, to allow for easy identification of the tract representing location of tetrodes and MFB electrodes, and then the brain was removed and post-fixed for another 24h. Last, the brain was cryoprotected in 30% sucrose in PBS. Frozen sections were cut coronally with a sliding microtome at a thickness of 40μm and split into 6 evenly spaced series.

6E10.: One series of sections was mounted on slides, incubated with 4% PFA (in PBS) for 4min, and then rinsed with Tris-buffered saline (TBS). Next, slides were soaked in 70% formic acid for 8–15min. After rinsing in TBS, slides were incubated in 0.1% Triton-X in TBS for 15min, followed by 0.1% Triton-X and 2% bovine serum albumin (BSA) in TBS for 30min. Sections were incubated with anti-β-amyloid 1–16 (mouse, clone 6E10, Biolegend) 1:1000 and anti-NeuN (polyclonal, rabbit, Milipore) in 0.1% Triton-X and 2% BSA in TBS for 2 days. After rinsing with TBS, slides were soaked in 0.1% Triton-X in TBS for 15min, followed again by 0.1% Triton-X and 2% BSA in TBS for 30min. Staining was visualized with anti-mouse-alexa-488 (1:1000) and anti-rabbit-alexa-594 (1:500) in 0.1% Triton-X and 2% BSA in TBS for 5–6h. Slides were coverslipped after being rinsed with TBS. Whole slides were imaged as described below, then the coverslip was removed and DAPI (0.01mg/ml) was added before the slides were re-coverslipped and reimaged. Except for β-Amyloid 1–16 as noted above, histology was performed on free-floating sections. Sections are permeabilized in 0.3% Triton-X and blocked in 3% Goat Serum in TBS, then incubated in primaries antibodies.

M78.: Sections were rinsed twice in PBS, then blocked in PBS containing 0.3% Triton X and 3% goat serum. Sections were incubated for two days with 0.3μg/ml anti-MOC78 (monoclonal, rabbit, abcam 205341) in PBS containing 0.3% Triton-X and 0.02% sodium azide. Next, sections were rinsed with PBS and 0.3% Triton-X three times. Sections were then incubated in anti-rabbit-alexa-488 (goat, 1:500) in 0.3% Triton-X overnight. Sections were then rinsed with PBS and 0.3% Triton-X washes for 20min five times. Next, sections were incubated in anti-NeuN-Cy3 (polyclonal, rabbit, Milipore, ABN78C) 1:300 in PBS with 0.3% Triton-X and 0.02% sodium azide for 24h. Finally, sections were rinsed once with PBS containing 0.3% Triton-X, and twice with PBS. Sections were mounted with Vectashield containing DAPI and coverslipped and imaged.

M22.: Sections were rinsed twice in PBS, then blocked in PBS containing 0.3% Triton X and 3% goat serum. xSections were incubated for two days with 0.5μg/ml anti-M22 (rabbit) in PBS containing 0.3% Triton-X and 0.02% sodium azide. Next, sections were rinsed three times in PBS with 0.3% Triton-X. Then, sections were incubated in anti-rabbit-alexa-488 (goat) 1:500 PBS with 0.3% Triton-X and 0.02% sodium azide overnight. Sections were then rinsed five times with PBS and 0.3% Triton-X. Sections were then incubated overnight in anti-NeuN-Cy3 (polyclonal, rabbit, Millipore ABN78C) 1:300 PBS with 0.3% Triton-X and 0.02% sodium azide overnight. Next, sections were rinsed once with PBS and 0.3% Triton-X, and then rinsed twice with PBS. Sections were mounted with Vectashield containing DAPI, coverslipped and imaged.

Thioflavin S.: Anti-NeuN (1:1000), overnight, was followed by anti-rabbit-alexa-594 (1:500) for 5h. Sections were rinsed then immersed in a 1% Thioflavin S solution (Sigma) for 9min, rinsed in dH2O, destained in 70% Ethanol for 5min, rinsed in dH2O, and then transferred to TBS before mounting onto slides.

Phosphorylated tau.: Incubation in anti-Phosphorylated tau (1:500, monoclonal, mouse, Thermo Scientific) with anti-NeuN (1:1000) overnight was followed by secondary antibodies, anti-mouse-alexa-488 (1:1000) and anti-rabbit-alexa-594 (1:500) respectively, for 6h. Sections were rinsed and mounted onto slides.

Parvalbumin.: Sections were quenched in 0.3% H_2O_2 in PBS for 25 minutes, then blocked in 5% goat serum in 0.5% Triton-X TBS for 90min. Primary antibody (mouse anti-parvalbumin; Sigma Aldrich) 1:2000 was added for 2 days, followed by a biotinylated goat anti-mouse antibody (Sigma Aldrich) 1:500 for 90min both in TBS with 0.5% Triton-X. Following this, A and B form the standard Vectastain ABC kit (Vector Laboratories) 1:500 in PBS was added for 1h. Staining was developed using a DAB (3,3′-Diaminobenzidine tetrahydrochloride hydrate; Sigma Aldrich) solution containing 0.05% DAB and 0.015% H_2O_2 in TBS. Sections were rinsed in PBS and mounted onto slides. After air drying, slides were dehydrated in increasing concentration of alcohol, cleared with Hemo-De and coverslip with Fisher Chemical Permount™ Mounting Medium.

Image Acquisition.: Whole slides were scanned using a scanning microscope at 40x magnification (NanoZoomer Digital Pathology RS Hamamatu) or 20x magnification (Zeiss Axioimager M2).

Genotyping.: We received homozygous 3xTg-AD mice from Dr. Frank LaFerla's lab. We confirmed that all mice used in the experiment contained each transgene using conventional PCR. DNA was extracted from the tails of each mouse. Homozygosity was confirmed by cutting the PS1 PCR fragment with the *BstEII* restriction enzyme. Only the mutated human PS1 gene contains a *BstEII* cut site and will be cut. The absence of an uncut PCR product indicated that the mouse was indeed homozygous for the human PS1. The presence of overexpressed APP and Tau were also confirmed by PCR. The previously published primers were used for amplifying the PS1 transgene, APP and Tau [24].

QUANTIFICATION AND STATISTICAL ANALYSIS

Recording and Quantification

Sleep and LFP Analyses.: First, still periods were extracted from the rest sessions as described previously [25, 74]. The raw position data from each video frame was smoothed by convolution of both x and y position data with a normalized Gaussian function (standard deviation of 120 video frames). After smoothing, the instantaneous velocity was found by taking the difference in position between successive video frames. An epoch during which the velocity was constantly below 0.78pixels/s (~0.19cm/s) for more than 2min was considered a stillness period. All analyses of rest sessions were limited to these stillness periods. SWS and REM sleep were distinguished using K-means clustering of the theta/delta power ratio extracted from the CA1 pyramidal layer LFP recorded during the stillness

periods, as is common for assessing memory replay [Figure 1B; 2–8, 57] and has been validated [143]. Only SWS periods were included in the analysis. DWTs, which correspond to cortical down states [75], were detected by digitally filtering the LFP trace from a representative cortical electrode in the 0.5–4Hz range and detecting the peaks in the inverted signal that exceeded a mean +1.5SD threshold. SWRs were detected from the hippocampal CA1 field LFP digitally filtered in the 75–300Hz range, determined a priori, and consistent with a literature review of common frequency ranges [10–16]. Events with peaks >6SD above the mean and duration 20–100ms were considered SWRs. The SWR duration included the contiguous periods surrounding the peak and exceeding 2SD above the mean. The SWR detection accuracy was visually validated on a subset of each analyzed dataset. This visual validation process caused us to adjust the SWR detection criteria for two (one NonTg, one 3xTg-AD) mice. For these mice events with peaks >7SD were used instead. Making this adjustment ensured that a similar signal to noise ratio was applied to all mice. In order to assess hippocampal-PC interactions, SWRs were cross-correlated with DWTs, and the SWR count binned (bin size 16.67ms - time bin of 100ms divided by 6x compression factor) as a function of position in time from the DWT was then z-scored. Since timing of the peak SWRxDWT correlation sometimes appears in slightly different time bins across animals and sessions (Figure S2), the peak value was compared irrespective of the precise position in time. Sleep spindles were detected on the same cortical electrode as DWT's. The raw LFP signal was digitally filtered in 8–18Hz range, followed by rectifying and z-scoring of the resulting signal. Sleep spindles were defined as the time windows with peaks >3.5SD above the mean and duration of 0.5–3s. Spindle duration was defined as the contiguous window around the spindle peak with envelope amplitude >2SD above the mean. Spindle onset and offset were defined as the first and the last timepoints of individual spindle events. Raw LFP in the window +/−2s surrounding the detected DWT was bandpass-filtered in spindle range (8–18Hz) and the peak of filtered signal was located. The delta-spindle coupling phase was defined as the phase of delta wave that coincided with spindle peak. The circular mean of delta-spindle coupling phases was calculated for each individual sleep epoch, using the circ_mean.m function from Matlab Circular Statistic Toolbox [144].

Template Matching.: We performed *template matching* analysis as was done previously to show the simultaneous reactivation of isolated single cell ensembles in the medial prefrontal cortex [74, 145] and that we applied more recently to MUA in PC [25]. The criteria for the inclusion of a dataset in the template matching analysis was at least 20min of stillness and 600DWTs during both *pre-task-sleep* and *post-task-sleep*, and at least 10 complete trials for VM (or at least 8 complete trials for the real-world spatial reorientation task). Template matrices (number of tetrodes x number of time bins; Figure 2A) were generated from the trial-averaged MUA template extracted from a 2s/trial windows that preceded the arrival at the reward site and binned (100ms binsize). Previous research in single cell template matching found that 100ms was the ideal bin size [74, 146]. The time window was chosen based on evidence that reactivation of the hippocampal activity patterns is more prominent for the task phase immediately preceding the reward [25, 76, 86, 147, 148]. However, to ensure that this bin size was ideal for our data we also assessed template matching with 200ms and 500ms bin sizes. For both these bin sizes, template matching dropped to about chance levels for all compression factors. In addition, when we assessed 50ms bin sizes,

activity was too sparse to find template matches during sleep. This assessment is in line with reports of template matching using isolated single unit activity [74, 146], where a 100ms bin was deemed optimal for capturing task-related neuronal dynamics and identical to what we used previously [25]. In order to eliminate tetrodes with sparse and/or poorly approach-modulated activity, only the tetrodes with average reward approach period MUA >1Hz and reward approach period binned spike train coefficient of variation >0.25 were included in the template. Coefficient of variation was calculated over twenty 100ms time bins. Only the templates containing ≥6 tetrodes localized in PC were retained. To eliminate the influence of signal amplitude variability between tetrodes, the binned signal was z-scored for each tetrode separately.

Due to the time-compressed nature of re-activation reported previously for single-cell [73, 74, 149] and MUA [25], we performed template matching for several evenly spaced compression factors: 'no-compression', 4x, 6x, 8x, and 10x. All of the template matching analyses were limited to SWS periods. Signal from the SWS periods was processed in the same way as for behavioral templates, except that the bin size was adjusted according to the compression factor (bin size=100ms/compression factor; e.g. for the 4x compression, the sleep bin size=25ms), to capture the compressed nature of neural reactivation during sleep.

To test the matching of a given template and the pattern of activity during sleep *(matching significance)*, and to identify the ideal compression factor for mice, we employed an approach identical to our previous work in rats [25]. First, each template was shuffled repeatedly to generate 100 *shuffled templates*. The shuffling procedure consisted of randomly permuting the position of each column in the template (*population vector*), preserving the overall activity levels and instantaneous correlations between the signals on different tetrodes, but scrambling the sequential patterns. A Pearson correlation coefficient was calculated between each template and the series of *candidate matches*, generated by sliding the template-size window over the SWS epochs. This resulted in a matrix of Pearson correlation coefficients r, where the element $r^{i,j}$ corresponded to the correlation coefficient between the i-th template and j-th candidate match. The correlation matrices were z-scored across individual time bins (columns), and the resulting z-score values reflected the template similarity to the corresponding sleep segment at the given time step, relative to the distribution that included the original and 100 shuffled templates. Z-score values above 3 were considered *matches* [25].

For comparison of template matching between the *pre-task-sleep* and *post-task-sleep*, *match percentage* was calculated by dividing the number of matches by the number of SWS time bins for each sleep epoch. For comparisons between the original and shuffled templates, means and distributions of z-score values obtained from the original and shuffled templates were compared within epoch. For the DWT-triggered template matching, the original template z-score traces +/1s around each DWT were averaged, obtaining the event-triggered averaged z-score for a given sleep epoch. The peri-event reactivation strength was defined as the maximum averaged event-triggered z-score value within +/−0.7s window surrounding detected event.

Statistical Analyses—Statistical comparisons were performed using two-way repeated measures ANOVAs (genotype x sleep session or genotype x day of behavior), paired t-tests (used when RMANOVA was not possible, for example due to imbalanced data sets), and chi-square analyses. For all statistical analyses, $p<0.05$ was considered significant after a Bonferroni correction for multiple comparisons was applied (when appropriate). Bonferroni corrected critical values are only shown for Bonferroni corrections that shift an uncorrected significant p-value to non-significant and not when the statistical result remains significant after Bonferroni correction. Statistical analyses were performed using Matlab Statistics and Circular Statistics toolboxes [144], StatView (SAS Institute Inc.) and Sigma Plot (Systat Software Inc.). Distributions of session-level circular means between groups for delta-wave phase relationship analyses were compared using the Watson-Williams test (ww_test function from Circular Statistic Toolbox).

Supplementary Material

Refer to Web version on PubMed Central for supplementary material.

Acknowledgements:

This research was supported by grants from NIA AG049090 to A.A.W. and B.L.M. was supported through DARPA HR0011-18-2-0021, NSERC Grant RGPIN-2017-03857 and Canadian Institutes of Health Research (CIHR) grant PJT 156040. We thank Frank LaFerla for 3xTg-AD mice.

References

1. Rosenzweig ES, Redish AD, McNaughton BL, and Barnes CA (2003). Hippocampal map realignment and spatial learning.[see comment]. Nature Neuroscience 6, 609–615. [PubMed: 12717437]
2. Buzsáki G, Buhl DL, Harris KD, Csicsvari J, Czéh B, and Morozov A (2003). Hippocampal network patterns of activity in the mouse. Neuroscience 116, 201–211. [PubMed: 12535953]
3. Grosmark Andres D., Mizuseki K, Pastalkova E, Diba K, and Buzsáki G (2012). REM Sleep Reorganizes Hippocampal Excitability. Neuron 75, 1001–1007. [PubMed: 22998869]
4. Lansink CS, Goltstein PM, Lankelma JV, Joosten RNJMA, McNaughton BL, and Pennartz CMA (2008). Preferential Reactivation of Motivationally Relevant Information in the Ventral Striatum. The Journal of Neuroscience 28, 6372–6382. [PubMed: 18562607]
5. Mizuseki K, Diba K, Pastalkova E, and Buzsáki G (2011). Hippocampal CA1 pyramidal cells form functionally distinct sublayers. Nature neuroscience 14, 1174. [PubMed: 21822270]
6. Mizuseki K, Sirota A, Pastalkova E, and Buzsáki G (2009). Theta Oscillations Provide Temporal Windows for Local Circuit Computation in the Entorhinal-Hippocampal Loop. Neuron 64, 267–280. [PubMed: 19874793]
7. Sirota A, Montgomery S, Fujisawa S, Isomura Y, Zugaro M, and Buzsáki G (2008). Entrainment of Neocortical Neurons and Gamma Oscillations by the Hippocampal Theta Rhythm. Neuron 60, 683–697. [PubMed: 19038224]
8. Stan Leung L (1998). Generation of Theta and Gamma Rhythms in the Hippocampus. Neuroscience & Biobehavioral Reviews 22, 275–290. [PubMed: 9579318]
9. Dragoi G, Carpi D, Recce M, Csicsvari J, and Buzsáki G (1999). Interactions between Hippocampus and Medial Septum during Sharp Waves and Theta Oscillation in the Behaving Rat. The Journal of Neuroscience 19, 6191–6199. [PubMed: 10407055]
10. Jadhav Shantanu P., Rothschild G, Roumis Demetris K., and Frank Loren M. (2016). Coordinated Excitation and Inhibition of Prefrontal Ensembles during Awake Hippocampal Sharp-Wave Ripple Events. Neuron 90, 113–127. [PubMed: 26971950]

11. Maier N, Nimmrich V, and Draguhn A (2003). Cellular and Network Mechanisms Underlying Spontaneous Sharp Wave-Ripple Complexes in Mouse Hippocampal Slices. The Journal of physiology 550, 873–887. [PubMed: 12807984]
12. Nimmrich V, Maier N, Schmitz D, and Draguhn A (2005). Induced sharp wave-ripple complexes in the absence of synaptic inhibition in mouse hippocampal slices. The Journal of physiology 563, 663–670. [PubMed: 15661820]
13. Oliva A, Fernández-Ruiz A, Buzsáki G, and Berényi A (2016). Role of Hippocampal CA2 Region in Triggering Sharp-Wave Ripples. Neuron 91, 1342–1355. [PubMed: 27593179]
14. Roux L, Hu B, Eichler R, Stark E, and Buzsáki G (2017). Sharp wave ripples during learning stabilize the hippocampal spatial map. Nature Neuroscience 20, 845. [PubMed: 28394323]
15. van de Ven GM, Trouche S, McNamara CG, Allen K, and Dupret D (2016). Hippocampal Offline Reactivation Consolidates Recently Formed Cell Assembly Patterns during Sharp Wave-Ripples. Neuron 92, 968–974. [PubMed: 27840002]
16. Yamamoto J, and Tonegawa S (2017). Direct Medial Entorhinal Cortex Input to Hippocampal CA1 Is Crucial for Extended Quiet Awake Replay. Neuron 96, 217–227.e214. [PubMed: 28957670]
17. McDade E, and Bateman RJ (2017). Stop Alzheimer's before it starts. Nature 547, 153–155. [PubMed: 28703214]
18. Henderson VW, Mack W, and Williams B (1989). Spatial disorientation in Alzheimer's disease. Archives of Neurology 46, 391–394. [PubMed: 2705898]
19. Weintraub S, Wicklund AH, and Salmon DP (2012). The Neuropsychological Profile of Alzheimer Disease. Cold Spring Harbor Perspectives in Medicine 2.
20. Allison SL, Fagan AM, Morris JC, and Head D (2016). Spatial Navigation in Preclinical Alzheimer's Disease. Journal of Alzheimer's disease : JAD 52, 77–90. [PubMed: 26967209]
21. Attar A, Liu T, Chan W-TC, Hayes J, Nejad M, Lei K, and Bitan G (2013). A Shortened Barnes Maze Protocol Reveals Memory Deficits at 4-Months of Age in the Triple-Transgenic Mouse Model of Alzheimer's Disease. PLoS ONE 8, e80355. [PubMed: 24236177]
22. Liu B, Frost JL, Sun J, Fu H, Grimes S, Blackburn P, and Lemere CA (2013). MER5101, a Novel Aβ1–15:DT Conjugate Vaccine, Generates a Robust Anti-Aβ Antibody Response and Attenuates Aβ Pathology and Cognitive Deficits in APPswe/PS1ΔE9 Transgenic Mice. The Journal of Neuroscience 33, 7027–7037. [PubMed: 23595760]
23. Marlatt M, Potter M, Bayer T, Praag H, and Lucassen P (2013). Prolonged Running, not Fluoxetine Treatment, Increases Neurogenesis, but does not Alter Neuropathology, in the 3xTg Mouse Model of Alzheimer's Disease In Neurogenesis and Neural Plasticity, Volume 15, Belzung C and Wigmore P, eds. (Springer Berlin Heidelberg), pp. 313–340.
24. Stimmell AC, Baglietto-Vargas D, Moseley SC, Lapointe V, Thompson LM, LaFerla FM, McNaughton BL, and Wilber AA (2019). Impaired Spatial Reorientation in the 3xTg-AD Mouse Model of Alzheimer's Disease. Scientific Reports 9, 1311. [PubMed: 30718609]
25. Wilber AA, Skelin I, Wu W, and McNaughton BL (2017). Laminar Organization of Encoding and Memory Reactivation in the Parietal Cortex. Neuron 95, 1406–1419.e1405. [PubMed: 28910623]
26. Maingret N, Girardeau G, Todorova R, Goutierre M, and Zugaro M (2016). Hippocampocortical coupling mediates memory consolidation during sleep. Nature Neuroscience 19, 959. [PubMed: 27182818]
27. Ji D, and Wilson MA (2006). Coordinated memory replay in the visual cortex and hippocampus during sleep. Nature Neuroscience 10, 100. [PubMed: 17173043]
28. Oess T, Krichmar JL, and Rohrbein F (2017). A Computational Model for Spatial Navigation Based on Reference Frames in the Hippocampus, Retrosplenial Cortex, and Posterior Parietal Cortex. Frontiers in neurorobotics 11, 4. [PubMed: 28223931]
29. McNaughton BL, Knierim JJ, and Wilson MA (1995). Vector encoding and the vestibular foundations of spatial cognition: Neurophysiological and computational mechanisms In The Cognitive Neurosciences, Gazzaniga MS, ed. (Cambridge: The MIT Press), pp. 585–595.
30. Byrne P, Becker S, and Burgess N (2007). Remembering the past and imagining the future: a neural model of spatial memory and imagery. Psychological review 114, 340–375. [PubMed: 17500630]

31. Clark BJ, Simmons CM, Berkowitz LE, and Wilber AA (2018). The retrosplenial-parietal network and reference frame coordination for spatial navigation. Behav Neurosci 132, 416–429. [PubMed: 30091619]
32. Jarrard LE (1993). On the role of the hippocampus in learning and memory in the rat. Behavioral and Neural Biology 60, 9–26. [PubMed: 8216164]
33. Kolb B, Buhrmann K, McDonald R, and Sutherland RJ (1994). Dissociation of the Medial Prefrontal, Posterior Parietal, and Posterior Temporal Cortex for Spatial Navigation and Recognition Memory in the Rat. Cerebral Cortex 4, 664–680. [PubMed: 7703691]
34. Morris RGM, Garrud P, Rawlins JNP, and O'Keefe J (1982). Place navigation impaired in rats with hippocampal lesions. Nature 297, 681. [PubMed: 7088155]
35. Nitz DA (2012). Spaces within spaces: rat parietal cortex neurons register position across three reference frames. Nature Neuroscience 15, 1365–1367. [PubMed: 22960933]
36. Pai MC, and Yang YC (2013). Impaired translation of spatial representation in young onset Alzheimer's disease patients. Current Alzheimer research 10, 95–103. [PubMed: 23036016]
37. Rogers JL, and Kesner RP (2006). Lesions of the dorsal hippocampus or parietal cortex differentially affect spatial information processing. Behavioral Neuroscience 120, 852–860. [PubMed: 16893291]
38. Sherrill KR, Erdem UM, Ross RS, Brown TI, Hasselmo ME, and Stern CE (2013). Hippocampus and Retrosplenial Cortex Combine Path Integration Signals for Successful Navigation. The Journal of Neuroscience 33, 19304–19313. [PubMed: 24305826]
39. Tu S, Spiers HJ, Hodges JR, Piguet O, and Hornberger M (2017). Egocentric versus Allocentric Spatial Memory in Behavioral Variant Frontotemporal Dementia and Alzheimer's Disease. J Alzheimers Dis 59, 883–892. [PubMed: 28697554]
40. Whitlock Jonathan R., Pfuhl G, Dagslott N, Moser M-B, and Moser Edvard I. (2012). Functional Split between Parietal and Entorhinal Cortices in the Rat. Neuron 73, 789–802. [PubMed: 22365551]
41. Wilber AA, Clark BJ, Forster TC, Tatsuno M, and McNaughton BL (2014). Interaction of egocentric and world-centered reference frames in the rat posterior parietal cortex. J Neurosci 34, 5431–5446. [PubMed: 24741034]
42. Aguirre GK, and D'Esposito M (1999). Topographical disorientation: a synthesis and taxonomy. Brain 122, 1613–1628. [PubMed: 10468502]
43. Jacobs HIL, Van Boxtel MPJ, Jolles J, Verhey FRJ, and Uylings HBM (2012). Parietal cortex matters in Alzheimer's disease: An overview of structural, functional and metabolic findings. Neuroscience & Biobehavioral Reviews 36, 297–309.
44. Kunz L, Schroder TN, Lee H, Montag C, Lachmann B, Sariyska R, Reuter M, Stirnberg R, Stocker T, Messing-Floeter PC, et al. (2015). Reduced grid-cell-like representations in adults at genetic risk for Alzheimer's disease. Science (New York, N.Y.) 350, 430–433.
45. Morbelli S, Drzezga A, Perneczky R, Frisoni GB, Caroli A, van Berckel BNM, Ossenkoppele R, Guedj E, Didic M, Brugnolo A, et al. (2012). Resting metabolic connectivity in prodromal Alzheimer's disease. A European Alzheimer Disease Consortium (EADC) project. Neurobiology of Aging 33, 2533–2550. [PubMed: 22365486]
46. Wang Y, Chen K, Yao L, Jin Z, Guo X, and the Alzheimer's Disease Neuroimaging, I. (2013). Structural Interactions within the Default Mode Network Identified by Bayesian Network Analysis in Alzheimer's Disease. PLoS ONE 8, e74070. [PubMed: 24015315]
47. Song Z, McDonough IM, Liu P, Lu H, and Park DC (2016). Cortical amyloid burden and age moderate hippocampal activity in cognitively-normal adults. NeuroImage. Clinical 12, 78–84. [PubMed: 27408792]
48. Mormino EC, Brandel MG, Madison CM, Marks S, Baker SL, and Jagust WJ (2012). Abeta Deposition in aging is associated with increases in brain activation during successful memory encoding. Cerebral cortex (New York, N.Y. : 1991) 22, 1813–1823.
49. Cacucci F, Yi M, Wills TJ, Chapman P, and O'Keefe J (2008). Place cell firing correlates with memory deficits and amyloid plaque burden in Tg2576 Alzheimer mouse model. Proceedings of the National Academy of Sciences 105, 7863–7868.

50. Huijbers W, Mormino EC, Wigman SE, Ward AM, Vannini P, McLaren DG, Becker JA, Schultz AP, Hedden T, Johnson KA, et al. (2014). Amyloid deposition is linked to aberrant entorhinal activity among cognitively normal older adults. The Journal of neuroscience : the official journal of the Society for Neuroscience 34, 5200–5210. [PubMed: 24719099]
51. De Gennaro L, Gorgoni M, Reda F, Lauri G, Truglia I, Cordone S, Scarpelli S, Mangiaruga A, D'atri A, Lacidogna G, et al. (2017). The Fall of Sleep K-Complex in Alzheimer Disease. Scientific Reports 7, 39688. [PubMed: 28045040]
52. Eichenbaum H (2010). Memory systems. Wiley Interdisciplinary Reviews: Cognitive Science 1, 478–490. [PubMed: 26271495]
53. Burke SN, Chawla MK, Penner MR, Crowell BE, Worley PF, Barnes CA, and McNaughton BL (2005). Differential Encoding of Behavior and Spatial Context in Deep and Superficial Layers of the Neocortex. Neuron 45, 667–674. [PubMed: 15748843]
54. Skelin I, Kilianski S, and McNaughton BL (2018). Hippocampal coupling with cortical and subcortical structures in the context of memory consolidation. Neurobiology of Learning and Memory.
55. Qin Y-L, McNaughton BL, Skaggs WE, and Barnes CA (1997). Memory Reprocessing in Corticocortical and Hippocampocortical Neuronal Ensembles. Philosophical Transactions: Biological Sciences 352, 1525–1533. [PubMed: 9368941]
56. Jadhav SP, Kemere C, German PW, and Frank LM (2012). Awake hippocampal sharp-wave ripples support spatial memory. Science (New York, N.Y.) 336, 1454–1458.
57. Girardeau G, Benchenane K, Wiener SI, Buzsaki G, and Zugaro MB (2009). Selective suppression of hippocampal ripples impairs spatial memory. Nat Neurosci 12, 1222–1223. [PubMed: 19749750]
58. Ego-Stengel V, and Wilson MA (2010). Disruption of ripple-associated hippocampal activity during rest impairs spatial learning in the rat. Hippocampus 20, 1–10. [PubMed: 19816984]
59. Staresina BP, Alink A, Kriegeskorte N, and Henson RN (2013). Awake reactivation predicts memory in humans. Proc Natl Acad Sci U S A.
60. Ciupek SM, Cheng J, Ali YO, Lu H-C, and Ji D (2015). Progressive Functional Impairments of Hippocampal Neurons in a Tauopathy Mouse Model. The Journal of Neuroscience 35, 8118–8131. [PubMed: 26019329]
61. Jones EA, Gillespie AK, Yoon SY, Frank LM, and Huang Y (2019). Early Hippocampal Sharp-Wave Ripple Deficits Predict Later Learning and Memory Impairments in an Alzheimer's Disease Mouse Model. Cell reports 29, 2123–2133. e2124. [PubMed: 31747587]
62. Witton J, Staniaszek LE, Bartsch U, Randall AD, Jones MW, and Brown JT (2016). Disrupted hippocampal sharp-wave ripple-associated spike dynamics in a transgenic mouse model of dementia. The Journal of physiology 594, 4615–4630. [PubMed: 25480798]
63. Gillespie AK, Jones EA, Lin YH, Karlsson MP, Kay K, Yoon SY, Tong LM, Nova P, Carr JS, Frank LM, et al. (2016). Apolipoprotein E4 Causes Age-Dependent Disruption of Slow Gamma Oscillations during Hippocampal Sharp-Wave Ripples. Neuron 90, 740–751. [PubMed: 27161522]
64. Mander BA, Winer JR, Jagust WJ, and Walker MP (2016). Sleep: A Novel Mechanistic Pathway, Biomarker, and Treatment Target in the Pathology of Alzheimer's Disease? Trends Neurosci. 39, 552–566. [PubMed: 27325209]
65. Van Erum J, Van Dam D, Sheorajpanday R, and De Deyn PP (2019). Sleep architecture changes in the APP23 mouse model manifest at onset of cognitive deficits. Behav. Brain Res 373, 112089. [PubMed: 31325518]
66. Billings LM, Oddo S, Green KN, McGaugh JL, and LaFerla FM (2005). Intraneuronal Abeta causes the onset of early Alzheimer's disease-related cognitive deficits in transgenic mice. Neuron 45, 675–688. [PubMed: 15748844]
67. Terry RD, Masliah E, Salmon DP, Butters N, DeTeresa R, Hill R, Hansen LA, and Katzman R (1991). Physical basis of cognitive alterations in alzheimer's disease: Synapse loss is the major correlate of cognitive impairment. Annals of neurology 30, 572–580. [PubMed: 1789684]
68. Flood DG, and Coleman PD (1990). Chapter 31 Chapter Hippocampal plasticity in normal aging and decreased plasticity in Alzheimer's disease In Progress in Brain Research, Volume Volume 83, Storm-Mathisen JZJ and Ottersen OP, eds. (Elsevier), pp. 435–443. [PubMed: 2203107]

69. Braak H, and Braak E (1991). Neuropathological stageing of Alzheimer-related changes. Acta neuropathologica 82, 239–259. [PubMed: 1759558]
70. Khan UA, Liu L, Provenzano FA, Berman DE, Profaci CP, Sloan R, Mayeux R, Duff KE, and Small SA (2014). Molecular drivers and cortical spread of lateral entorhinal cortex dysfunction in preclinical Alzheimer's disease. Nat Neurosci 17, 304–311. [PubMed: 24362760]
71. Mitchell TW, Mufson EJ, Schneider JA, Cochran EJ, Nissanov J, Han LY, Bienias JL, Lee VM, Trojanowski JQ, Bennett DA, et al. (2002). Parahippocampal tau pathology in healthy aging, mild cognitive impairment, and early Alzheimer's disease. Annals of neurology 51, 182–189. [PubMed: 11835374]
72. Mesulam MM (1999). Neuroplasticity Failure in Alzheimer's Disease: Bridging the Gap between Plaques and Tangles. Neuron 24, 521–529. [PubMed: 10595506]
73. Peyrache A, Khamassi M, Benchenane K, Wiener SI, and Battaglia FP (2009). Replay of rule-learning related neural patterns in the prefrontal cortex during sleep. Nat Neurosci 12, 919–926. [PubMed: 19483687]
74. Euston DR, Tatsuno M, and McNaughton BL (2007). Fast-Forward Playback of Recent Memory Sequences in Prefrontal Cortex During Sleep. Science (New York, N.Y.) 318, 1147–1150.
75. Battaglia FP, Sutherland GR, and McNaughton BL (2004). Local Sensory Cues and Place Cell Directionality: Additional Evidence of Prospective Coding in the Hippocampus. The Journal of Neuroscience 24, 4541–4550. [PubMed: 15140925]
76. Diba K, and Buzsaki G (2007). Forward and reverse hippocampal place-cell sequences during ripples. Nat Neurosci 10, 1241–1242. [PubMed: 17828259]
77. Stover KR, Campbell MA, Van Winssen CM, and Brown RE (2015). Analysis of motor function in 6-month-old male and female 3xTg-AD mice. Behavioural Brain Research 281, 16–23. [PubMed: 25486177]
78. Garvock-de Montbrun T, Fertan E, Stover K, and Brown RE (2019). Motor deficits in 16-month-old male and female 3xTg-AD mice. Behavioural Brain Research 356, 305–313. [PubMed: 30208295]
79. Roh JH, Huang Y, Bero AW, Kasten T, Stewart FR, Bateman RJ, and Holtzman DM (2012). Disruption of the sleep-wake cycle and diurnal fluctuation of beta-amyloid in mice with Alzheimer's disease pathology. Science translational medicine 4, 150ra122.
80. Clemens Z, Mölle M, Erőss L, Barsi P, Halász P, and Born J (2007). Temporal coupling of parahippocampal ripples, sleep spindles and slow oscillations in humans. Brain 130, 2868–2878. [PubMed: 17615093]
81. Helfrich RF, Mander BA, Jagust WJ, Knight RT, and Walker MP (2018). Old Brains Come Uncoupled in Sleep: Slow Wave-Spindle Synchrony, Brain Atrophy, and Forgetting. Neuron 97, 221–230.e224. [PubMed: 29249289]
82. Siapas AG, and Wilson MA (1998). Coordinated Interactions between Hippocampal Ripples and Cortical Spindles during Slow-Wave Sleep. Neuron 21, 1123–1128. [PubMed: 9856467]
83. Sirota A, Csicsvari J, Buhl D, and Buzsáki G (2003). Communication between neocortex and hippocampus during sleep in rodents. Proceedings of the National Academy of Sciences 100, 2065–2069.
84. Winer JR, Mander BA, Helfrich RF, Maass A, Harrison TM, Baker SL, Knight RT, Jagust WJ, and Walker MP (2019). Sleep as a potential biomarker of tau and β-amyloid burden in the human brain. The Journal of Neuroscience, 0503–0519.
85. Oddo S, Caccamo A, Shepherd JD, Murphy MP, Golde TE, Kayed R, Metherate R, Mattson MP, Akbari Y, and LaFerla FM (2003). Triple-Transgenic Model of Alzheimer's Disease with Plaques and Tangles: Intracellular Aβ and Synaptic Dysfunction. Neuron 39, 409–421. [PubMed: 12895417]
86. Foster DJ, and Wilson MA (2006). Reverse replay of behavioural sequences in hippocampal place cells during the awake state. Nature 440, 680–683. [PubMed: 16474382]
87. Lim AS, Kowgier M, Yu L, Buchman AS, and Bennett DA (2013). Sleep fragmentation and the risk of incident Alzheimer's disease and cognitive decline in older persons. Sleep 36, 1027–1032. [PubMed: 23814339]

88. Bliwise DL, Tinklenberg J, Yesavage JA, Davies H, Pursley AM, Petta DE, Widrow L, Guilleminault C, Zarcone VP, and Dement WC (1989). REM latency in Alzheimer's disease. Biological Psychiatry 25, 320–328. [PubMed: 2914155]

89. BONANNI E, MAESTRI M, TOGNONI G, FABBRINI M, NUCCIARONE B, MANCA ML, GORI S, IUDICE A, and MURRI L (2005). Daytime sleepiness in mild and moderate Alzheimer's disease and its relationship with cognitive impairment. Journal of Sleep Research 14, 311–317. [PubMed: 16120107]

90. Grace JB, Walker MP, and McKeith IG (2000). A comparison of sleep profiles in patients with dementia with Lewy bodies and Alzheimer's disease. International Journal of Geriatric Psychiatry 15, 1028–1033. [PubMed: 11113983]

91. Ju Y-ES, McLeland JS, Toedebusch CD, Xiong C, Fagan AM, Duntley SP, Morris JC, and Holtzman DM (2013). Sleep Quality and Preclinical Alzheimer DiseaseSleep Quality and Preclinical Alzheimer Disease. JAMA Neurology 70, 587–593. [PubMed: 23479184]

92. Liguori C, Mercuri NB, Izzi F, Romigi A, Cordella A, Sancesario G, and Placidi F (2017). Obstructive Sleep Apnea is Associated With Early but Possibly Modifiable Alzheimer's Disease Biomarkers Changes. Sleep 40.

93. Liguori C, Romigi A, Nuccetelli M, Zannino S, Sancesario G, Martorana A, Albanese M, Mercuri NB, Izzi F, Bernardini S, et al. (2014). Orexinergic System Dysregulation, Sleep Impairment, and Cognitive Decline in Alzheimer DiseaseOrexinergic Dysregulation in Alzheimer DiseaseOrexinergic Dysregulation in Alzheimer Disease. JAMA Neurology 71, 1498–1505. [PubMed: 25322206]

94. Mander BA, Winer JR, and Walker MP (2017). A restless night makes for a rising tide of amyloid. Brain 140, 2066–2069. [PubMed: 28899024]

95. Musiek ES, Xiong DD, and Holtzman DM (2015). Sleep, circadian rhythms, and the pathogenesis of Alzheimer Disease. Experimental &Amp; Molecular Medicine 47, e148.

96. Peter-Derex L, Yammine P, Bastuji H, and Croisile B (2015). Sleep and Alzheimer's disease. Sleep Medicine Reviews 19, 29–38. [PubMed: 24846773]

97. Rothman SM, and Mattson MP (2012). Sleep Disturbances in Alzheimer's and Parkinson's Diseases. NeuroMolecular Medicine 14, 194–204. [PubMed: 22552887]

98. Vitiello MV, Prinz PN, Williams DE, Frommlet MS, and Ries RK (1990). Sleep Disturbances in Patients With Mild-Stage Alzheimer's Disease. Journal of Gerontology 45, M131–M138. [PubMed: 2365965]

99. Yaffe K, Laffan AM, Harrison SL, Redline S, Spira AP, Ensrud KE, Ancoli-Israel S, and Stone KL (2011). Sleep-disordered breathing, hypoxia, and risk of mild cognitive impairment and dementia in older women. Jama 306, 613–619. [PubMed: 21828324]

100. Sprecher KE, Koscik RL, Carlsson CM, Zetterberg H, Blennow K, Okonkwo OC, Sager MA, Asthana S, Johnson SC, Benca RM, et al. (2017). Poor sleep is associated with CSF biomarkers of amyloid pathology in cognitively normal adults. Neurology 89, 445–453. [PubMed: 28679595]

101. Holth JK, Patel TK, and Holtzman DM (2017). Sleep in Alzheimer's Disease–Beyond Amyloid. Neurobiology of Sleep and Circadian Rhythms 2, 4–14. [PubMed: 28217760]

102. Varga AW, Wohlleber ME, Giménez S, Romero S, Alonso JF, Ducca EL, Kam K, Lewis C, Tanzi EB, Tweardy S, et al. (2016). Reduced Slow-Wave Sleep Is Associated with High Cerebrospinal Fluid Aβ42 Levels in Cognitively Normal Elderly. Sleep 39, 2041–2048. [PubMed: 27568802]

103. Ju Y-ES, Ooms SJ, Sutphen C, Macauley SL, Zangrilli MA, Jerome G, Fagan AM, Mignot E, Zempel JM, Claassen JAHR, et al. (2017). Slow wave sleep disruption increases cerebrospinal fluid amyloid-β levels. Brain 140, 2104–2111. [PubMed: 28899014]

104. Lucey BP, Hicks TJ, McLeland JS, Toedebusch CD, Boyd J, Elbert DL, Patterson BW, Baty J, Morris JC, and Ovod V (2018). Effect of sleep on overnight cerebrospinal fluid amyloid β kinetics. Annals of neurology 83, 197–204. [PubMed: 29220873]

105. Olsson M, Ärlig J, Hedner J, Blennow K, and Zetterberg H (2018). Sleep deprivation and cerebrospinal fluid biomarkers for Alzheimer's disease. Sleep 41, zsy025.

106. Boespflug EL, and Iliff JJ (2018). The Emerging Relationship Between Interstitial Fluid–Cerebrospinal Fluid Exchange, Amyloid-β, and Sleep. Biological Psychiatry 83, 328–336. [PubMed: 29279202]
107. Branger P, Arenaza-Urquijo EM, Tomadesso C, Mézenge F, André C, de Flores R, Mutlu J, de La Sayette V, Eustache F, Chételat G, et al. (2016). Relationships between sleep quality and brain volume, metabolism, and amyloid deposition in late adulthood. Neurobiology of Aging 41, 107–114. [PubMed: 27103523]
108. Yun C-H, Lee H-Y, Lee SK, Kim H, Seo HS, Bang S, Kim SE, Greve DN, Au R, and Shin C (2017). Amyloid burden in obstructive sleep apnea. Journal of Alzheimer's Disease 59, 21–29.
109. Sprecher KE, Bendlin BB, Racine AM, Okonkwo OC, Christian BT, Koscik RL, Sager MA, Asthana S, Johnson SC, and Benca RM (2015). Amyloid burden is associated with self-reported sleep in nondemented late middle-aged adults. Neurobiology of Aging 36, 2568–2576. [PubMed: 26059712]
110. Fagan AM, Mintun MA, Mach RH, Lee S-Y, Dence CS, Shah AR, LaRossa GN, Spinner ML, Klunk WE, Mathis CA, et al. (2006). Inverse relation between in vivo amyloid imaging load and cerebrospinal fluid Aβ42 in humans. Annals of neurology 59, 512–519. [PubMed: 16372280]
111. Cordone S, Annarumma L, Rossini PM, and De Gennaro L (2019). Sleep and β-Amyloid Deposition in Alzheimer Disease: Insights on Mechanisms and Possible Innovative Treatments. Frontiers in Pharmacology 10.
112. Lim ASP, Kowgier M, Yu L, Buchman AS, and Bennett DA (2013). Sleep Fragmentation and the Risk of Incident Alzheimer's Disease and Cognitive Decline in Older Persons. Sleep 36, 1027–1032. [PubMed: 23814339]
113. Ju Y-ES, Lucey BP, and Holtzman DM (2013). Sleep and Alzheimer disease pathology—a bidirectional relationship. Nature Reviews Neurology 10, 115. [PubMed: 24366271]
114. Colas D, London J, Gharib A, Cespuglio R, and Sarda N (2004). Sleep–wake architecture in mouse models for Down syndrome. Neurobiology of Disease 16, 291–299. [PubMed: 15193286]
115. Huitrón-Reséndiz S, Sánchez-Alavez M, Gallegos R, Berg G, Crawford E, Giacchino JL, Games D, Henriksen SJ, and Criado JR (2002). Age-independent and age-related deficits in visuospatial learning, sleep-wake states, thermoregulation and motor activity in PDAPP mice. Brain Research 928, 126–137. [PubMed: 11844479]
116. Jyoti A, Plano A, Riedel G, and Platt B (2010). EEG, Activity, and Sleep Architecture in a Transgenic AβPP swe/PSEN1 A246E Alzheimer's Disease Mouse. Journal of Alzheimer's Disease 22, 873–887.
117. Roh JH, Huang Y, Bero AW, Kasten T, Stewart FR, Bateman RJ, and Holtzman DM (2012). Disruption of the Sleep-Wake Cycle and Diurnal Fluctuation of β-Amyloid in Mice with Alzheimer's Disease Pathology. Science translational medicine 4, 150ra122–150ra122.
118. Schneider F, Baldauf K, Wetzel W, and Reymann KG (2014). Behavioral and EEG changes in male 5xFAD mice. Physiology & Behavior 135, 25–33. [PubMed: 24907698]
119. Wisor JP, Edgar DM, Yesavage J, Ryan HS, McCormick CM, Lapustea N, and Murphy GM (2005). Sleep and circadian abnormalities in a transgenic mouse model of Alzheimer's disease: A role for cholinergic transmission. Neuroscience 131, 375–385. [PubMed: 15708480]
120. Zhang B, Veasey SC, Wood MA, Leng LZ, Kaminski C, Leight S, Abel T, Lee VMY, and Trojanowski JQ (2005). Impaired Rapid Eye Movement Sleep in the Tg2576 APP Murine Model of Alzheimer's Disease with Injury to Pedunculopontine Cholinergic Neurons. The American Journal of Pathology 167, 1361–1369. [PubMed: 16251420]
121. Kent BA, Strittmatter SM, and Nygaard H (2018). Sleep and EEG power spectral analysis in three transgenic mouse models of Alzheimer's disease: APP/PS1, 3xTgAD, and Tg2576. Journal of Alzheimer's Disease, 1–12.
122. Koss DJ, Robinson L, Drever BD, Plucińska K, Stoppelkamp S, Veselcic P, Riedel G, and Platt B (2016). Mutant Tau knock-in mice display frontotemporal dementia relevant behaviour and histopathology. Neurobiology of Disease 91, 105–123. [PubMed: 26949217]
123. Cheng J, and Ji D (2013). Rigid firing sequences undermine spatial memory codes in a neurodegenerative mouse model. eLife 2, e00647. [PubMed: 23805379]

124. Teyler TJ, and DiScenna P (1986). The hippocampal memory indexing theory. Behavioral neuroscience 100, 147. [PubMed: 3008780]
125. Marshall L, and Born J (2007). The contribution of sleep to hippocampus-dependent memory consolidation. Trends in cognitive sciences 11, 442–450. [PubMed: 17905642]
126. Buzsáki G (1989). Two-stage model of memory trace formation: a role for "noisy" brain states. Neuroscience 31, 551–570. [PubMed: 2687720]
127. Nadel L, Samsonovich A, Ryan L, and Moscovitch M (2000). Multiple trace theory of human memory: Computational, neuroimaging, and neuropsychological results. Hippocampus 10, 352–368. [PubMed: 10985275]
128. Scoville W, and Milner B (1957). Loss of recent memory after bilateral hippocampal lesions. Journal of Neurology, Neurosurgery and Psychiatry 20, 11–21.
129. Kubie JL, Sutherland RJ, and Muller RU (1999). Hippocampal lesions produce a temporally graded retrograde amnesia on a dry version of the Morris swimming task. Psychobiology 27, 313–330.
130. Diekelmann S, and Born J (2010). The memory function of sleep. Nature Reviews Neuroscience 11, 114–126. [PubMed: 20046194]
131. Frankland PW, and Bontempi B (2005). The organization of recent and remote memories. Nature Reviews Neuroscience 6, 119–130. [PubMed: 15685217]
132. Latchoumane C-FV, Ngo H-VV, Born J, and Shin H-S (2017). Thalamic Spindles Promote Memory Formation during Sleep through Triple Phase-Locking of Cortical, Thalamic, and Hippocampal Rhythms. Neuron 95, 424–435.e426. [PubMed: 28689981]
133. Staresina BP, Bergmann TO, Bonnefond M, Van Der Meij R, Jensen O, Deuker L, Elger CE, Axmacher N, and Fell J (2015). Hierarchical nesting of slow oscillations, spindles and ripples in the human hippocampus during sleep. Nature neuroscience 18, 1679. [PubMed: 26389842]
134. Clemens Z, Mölle M, Erőss L, Jakus R, Rásonyi G, Halász P, and Born J (2011). Fine-tuned coupling between human parahippocampal ripples and sleep spindles. European Journal of Neuroscience 33, 511–520. [PubMed: 21138489]
135. Oddo S, Caccamo A, Shepherd JD, Murphy MP, Golde TE, Kayed R, Metherate R, Mattson MP, Akbari Y, and LaFerla FM (2003). Triple-transgenic model of Alzheimer's disease with plaques and tangles: intracellular Abeta and synaptic dysfunction. Neuron 39, 409–421. [PubMed: 12895417]
136. Clark JK, Furgerson M, Crystal JD, Fechheimer M, Furukawa R, and Wagner JJ (2015). Alterations in synaptic plasticity coincide with deficits in spatial working memory in presymptomatic 3xTg-AD mice. Neurobiology of learning and memory 125, 152–162. [PubMed: 26385257]
137. Rasch B, and Born J (2013). About sleep's role in memory. Physiological reviews 93, 681–766. [PubMed: 23589831]
138. Bliss TV, and Collingridge GL (1993). A synaptic model of memory: long-term potentiation in the hippocampus. Nature 361, 31–39. [PubMed: 8421494]
139. Roy DS, Arons A, Mitchell TI, Pignatelli M, Ryan TJ, and Tonegawa S (2016). Memory retrieval by activating engram cells in mouse models of early Alzheimer's disease. Nature 531, 508–512. [PubMed: 26982728]
140. Chang EH, Frattini SA, Robbiati S, and Huerta PT (2013). Construction of Microdrive Arrays for Chronic Neural Recordings in Awake Behaving Mice. JoVE, e50470. [PubMed: 23851569]
141. Molina LA, Needham MA, Mohajerani MH, and McNaughton BL (2016). Tablet based virtual reality system for research purposes: https://www.interphaser.com/ In Society for Neuroscinece. (San Diego, CA), pp. 1610–1611.
142. Harris KD, Henze DA, Csicsvari J, Hirase H, and Buzsáki G (2000). Accuracy of Tetrode Spike Separation as Determined by Simultaneous Intracellular and Extracellular Measurements. J. Neurophysiol 84, 401–414. [PubMed: 10899214]
143. Costa-Miserachs D, Portell-Cortés I, Torras-Garcia M, and Morgado-Bernal I (2003). Automated sleep staging in rat with a standard spreadsheet. Journal of Neuroscience Methods 130, 93–101. [PubMed: 14583408]
144. Berens P (2009). CircStat: a MATLAB toolbox for circular statistics. J Stat Softw 31, 1–21.

145. Louie K, and Wilson MA (2001). Temporally Structured Replay of Awake Hippocampal Ensemble Activity during Rapid Eye Movement Sleep. Neuron 29, 145–156. [PubMed: 11182087]

146. Johnson LA, Euston DR, Tatsuno M, and McNaughton BL (2010). Stored-Trace Reactivation in Rat Prefrontal Cortex Is Correlated with Down-to-Up State Fluctuation Density. The Journal of Neuroscience 30, 2650–2661. [PubMed: 20164349]

147. McNamara CG, Tejero-Cantero A, Trouche S, Campo-Urriz a N, and Dupret D (2014). Dopaminergic neurons promote hippocampal reactivation and spatial memory persistence. Nat Neurosci 17, 1658–1660. [PubMed: 25326690]

148. Singer AC, and Frank LM (2009). Rewarded outcomes enhance reactivation of experience in the hippocampus. Neuron 64, 910–921. [PubMed: 20064396]

149. Wilson MA, and McNaughton BL (1994). Reactivation of hippocampal ensemble memories during sleep. Science (New York, N.Y.) 265, 676–679.

- In 3xTg-AD mice, increased sleep may compensate for some impaired brain dynamics.
- Task-induced increased cortical-hippocampal coupling predicts spatial learning.
- Deficits in spatial learning and cortical-hippocampal coupling in 3xTg-AD mice.
- Spindle-Delta coupling deficits in cortex parallels cortical-hippocampal deficits.

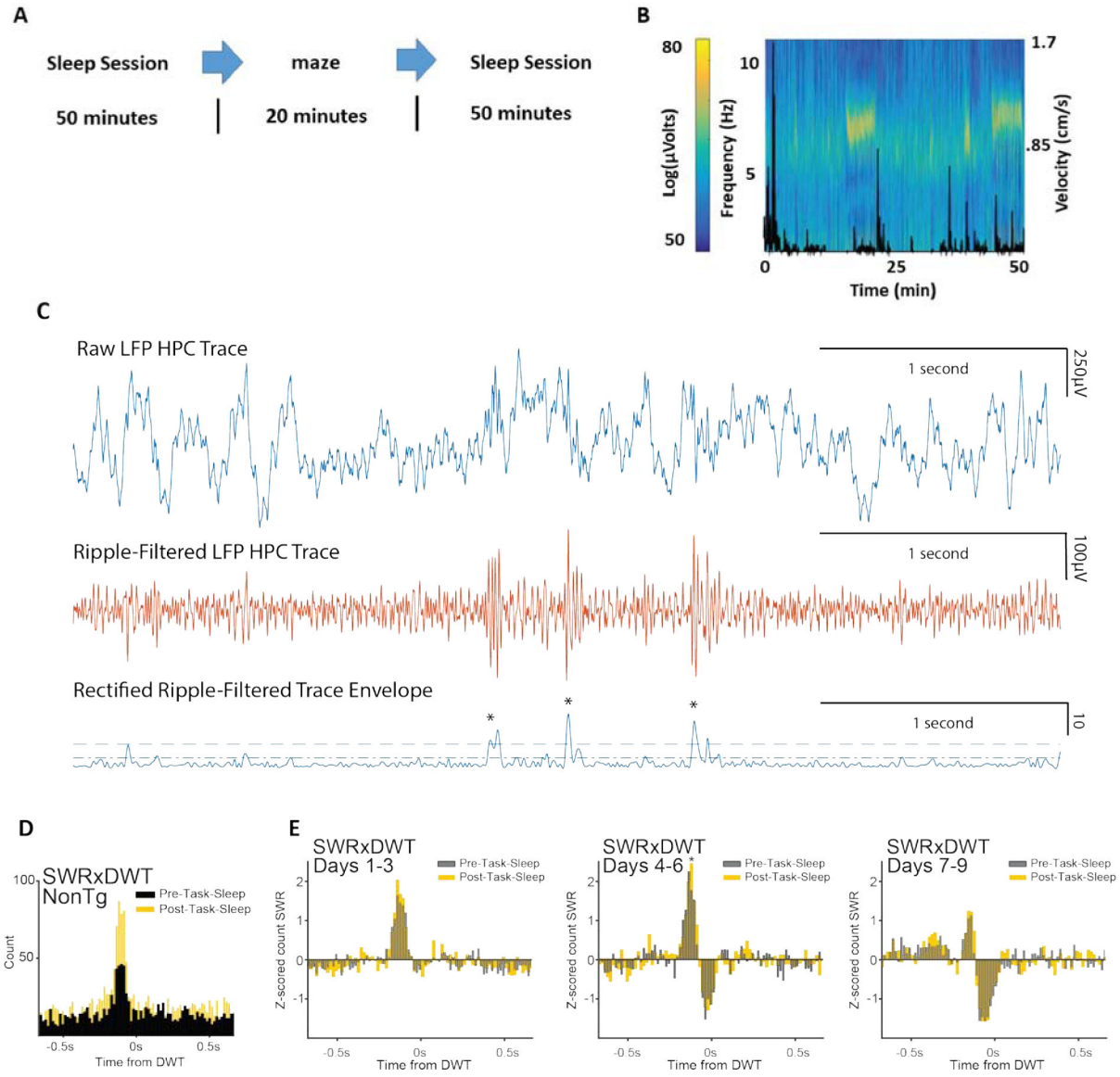

Figure 1. Hippocampal-cortical coupling is strong during early VM training.

A. Recording sessions started with *pre-task-sleep* session, followed by the task (real or virtual maze, or nose poke training), then *post-task-sleep* session. Sleep sessions were 50min each and task sessions lasted 20min for each daily recording session. **B**. Time frequency power spectrum for CA1 LFP overlaid with movement velocity (black line) illustrates contrast between slow wave sleep (SWS; low velocity & low theta power), REM sleep (low velocity & high theta), and awake [high velocity & low theta; 2, 3–8]. See also Supplemental Figure 1A. C. SWRs were detected from the CA1 local field potential (LFP; *top*) and digitally filtered in 75–300Hz (*middle*). An envelope was created from the z-scored filtered trace (*bottom*). Events with peaks >6SD (dashed line) above the mean and duration 20–100ms were considered SWRs. The SWR duration included the contiguous periods surrounding the peak and exceeding 2SD (dotted line) above the mean [9–16]. **D.** Cross-correlation between SWRs and DWTs for example data set shows increased post-task

(cream) coupling. **E.** Average z-scored SWR-DWT cross-correlation for all data sets in NonTg animals that met the inclusion criteria in days 1–3, 4–6, and 7–9 of the VM task. The average temporal correlation between hippocampal SWR and DWT decreases sharply after the first 6 days of VM training. The average peak of the cross-correlation exceeded 1SD in the positive direction for days 1–3 & 4–6, but not 7–9 and was significantly greater in *post-task-sleep* than *pre-task-sleep* for days 4–6 (*$p<0.05$). See also Figure S2 and Table S2

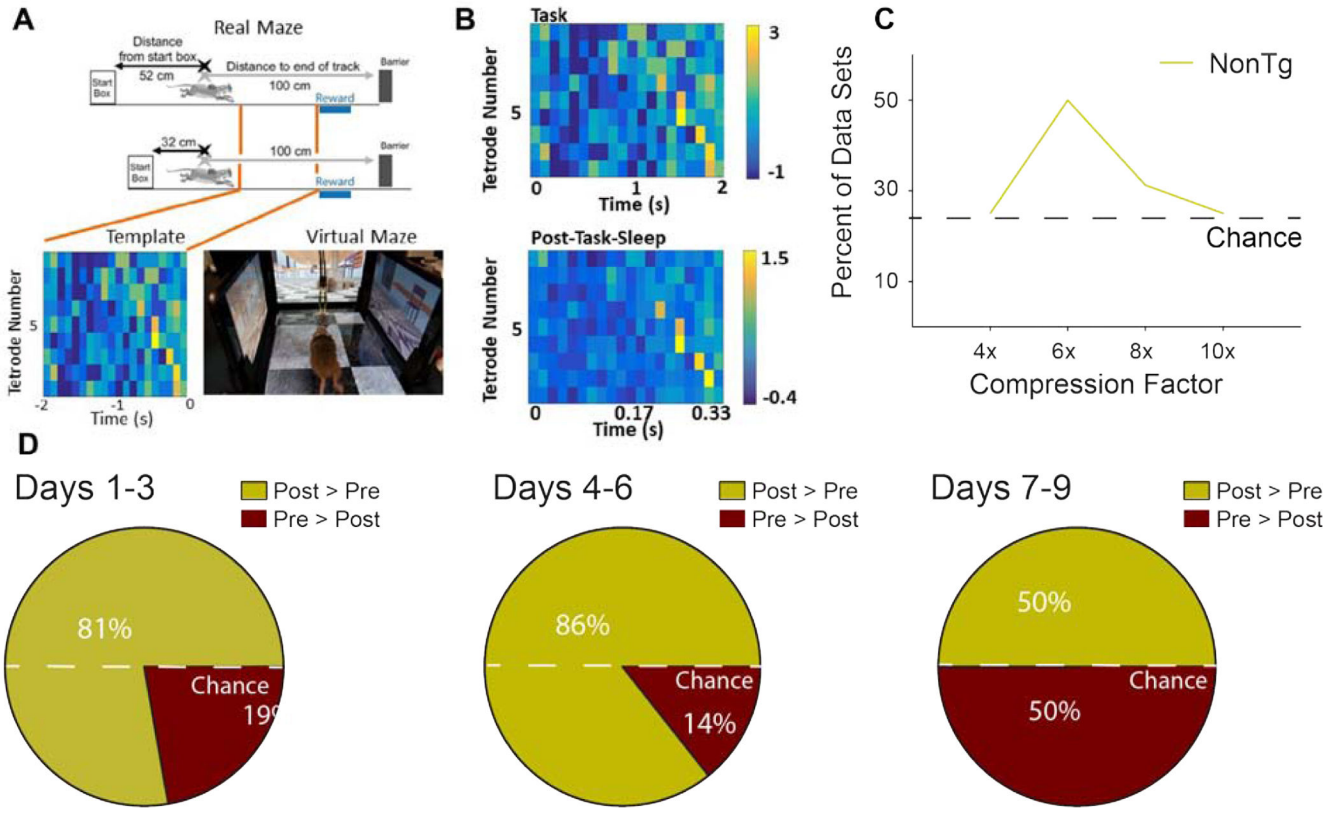

Figure 2 A. Memory replay measures suggest decreased reactivation strength after 6 days of VM training.

Top. The maze task includes an unmarked rewarded location (blue bar) that is fixed within the real or virtual room; however, the start position "moves" between trials. If only run in the long track configuration (*top*), the mouse could get position estimates from self-motion (black) and real or virtual room cues (gray); however, because there is a randomly selected set of track lengths (e.g., *bottom*), so only room cues provide accurate position information. Adapted from [1]. *Bottom Left*. A template is constructed by averaging MUA across trials for each tetrode (rows) for the 2s period where the mouse approaches the reward zone on correct response trials. *Bottom Right*. We developed a mouse VM system. Distal cues surround the virtual arena. This a novel tablet-based control mechanism in which each mouse extremity is sensed just like a finger swipe on a phone. This results in many more trials (343% increase) on a 2D VM. **B.** A *task template* is constructed (NonTg mouse example; *top*). Next, the similarity is computed between this template and neural activity during a sliding window advanced one time-bin at a time over SWS periods. Due to the compressed nature of memory reactivation, strong matches are only obtained when bin sizes are adjusted by a compression factor (e.g., for 6x *bottom* 0.333s sleep = 2s task). The top 100 matches were averaged to illustrate the strong correspondence between task template and activity patterns during *post-task-sleep*. Warm colors represent higher MUA z-score for that time bin. **C.** The percent of data sets for which template matches are greater in *post-task-sleep* and also greater than non-compressed data for NonTg (cream line) mice indicates a peak in template matches for the 6x compression factor. **D.** The proportion of data sets in which the proportion of 6x compression factor template matches was larger in *post-task-*

sleep for all NonTg mouse data sets that met inclusion criteria for days 1–3, 4–6, and 7–9 of VM training, Template matching in PC parallels the SWR-DWT coupling strength time course and also falls off sharply in days 7–9. See also Table S2.

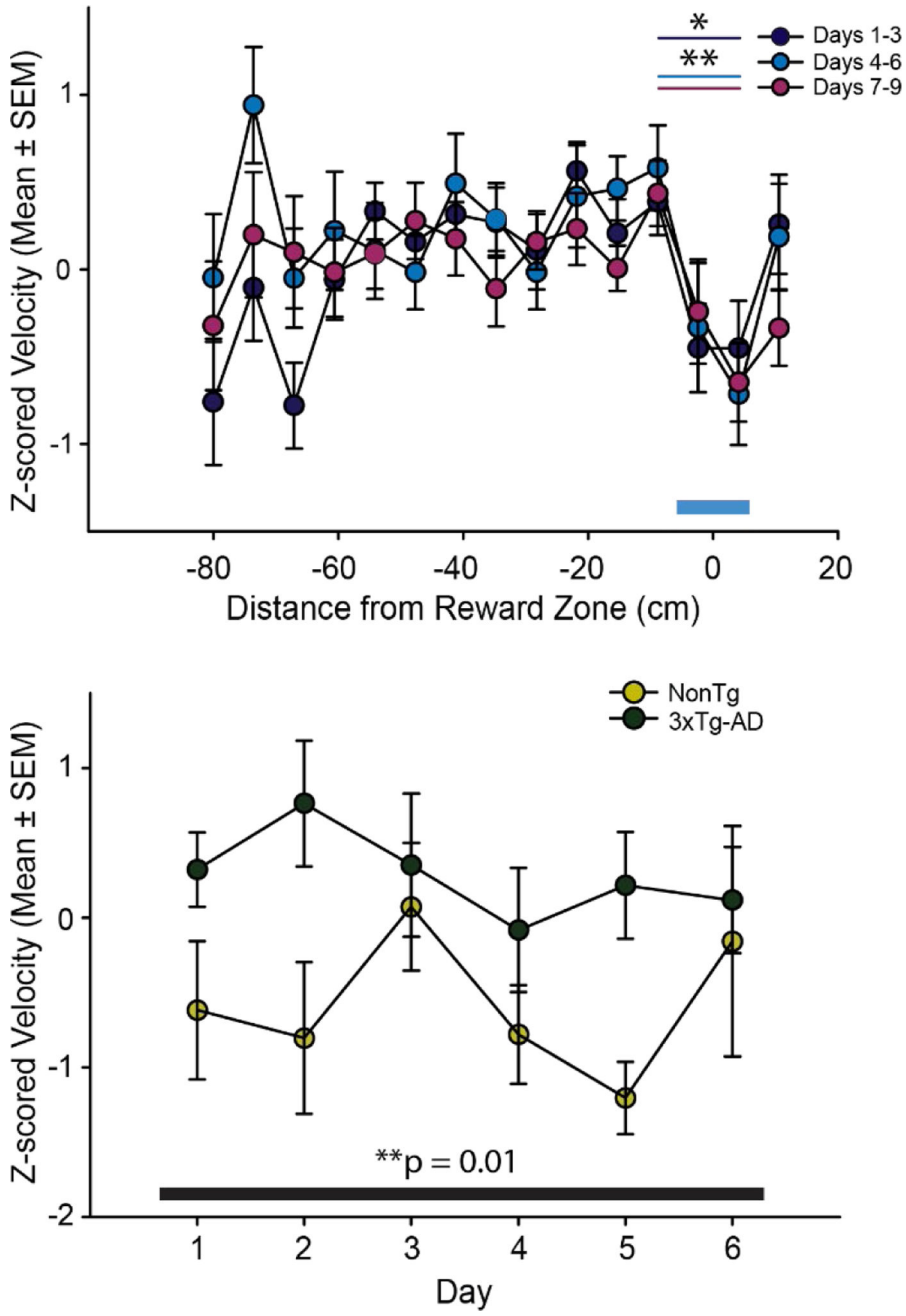

Figure 3. Impaired Spatial Learning and Memory on the VM.

Top. Average Z-scored velocity Mean±SEM as a function of distance from reward zone (blue bar) for NonTg mice for days 1–3 (navy), days 4–6 (blue) and days 7–9 (pink). NonTg mice slowed in reward zone, indicating knowledge of reward zone location based on maze cues in the virtual room (ps≤0.05). *Bottom.* Velocity in reward zone for NonTg (cream) and 3xTg-AD (green) mice during the first 6 days of behavior. 3xTg-AD mice slowed significantly less in reward zone with no main effect of day (p=0.01). See also Table S2.

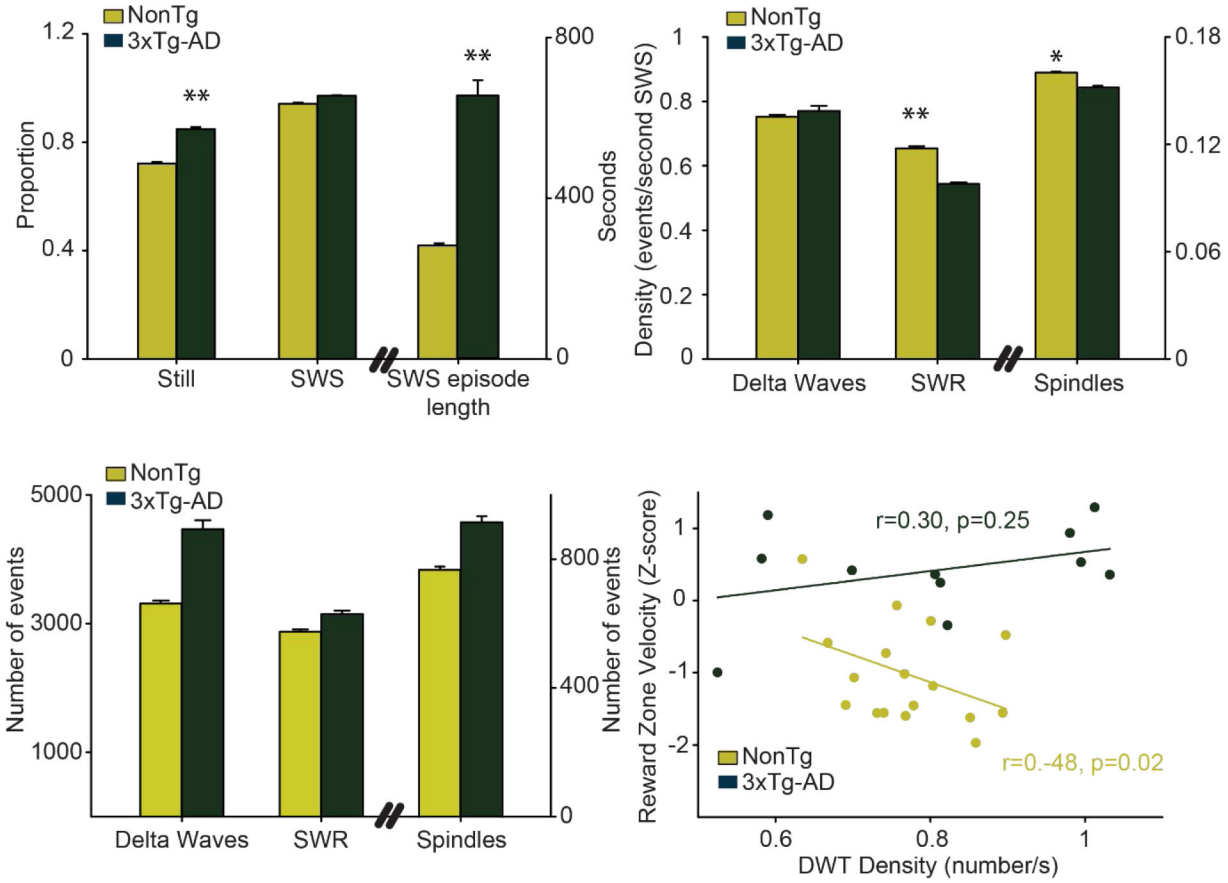

Figure 4. Sleep changes in AD mice compensate for a decreased SWR density.

Top Left. Mean±SEM proportion of stillness and SWS, and SWS episode length for NonTg (cream) and 3xTg-AD (green) mice. 3xTg-AD mice spent a greater proportion of the sleep session still and had increased SWS episode average length. *Top Right*. Density of DWTs, SWRs, and spindles from SWS. 3xTg-AD mice had decreased SWR and spindle density. *Bottom left*. Total number of SWRs, DWTs, and spindles. *Bottom Right*. Higher DWT rate was a significant predictor of behavioral performance (z-scored velocity in the reward zone) the following day for NonTg (*cream*) but not for 3xTg-AD (*green*) mice. There was not a significant effect of sleep phase or interaction with genotype, so *pre-* and *post-task-sleep* were combined for illustrative simplicity. * $p \leq 0.05$ ** $p \leq 0.01$. See also Figures S1, S3 and S4 and Table S2.

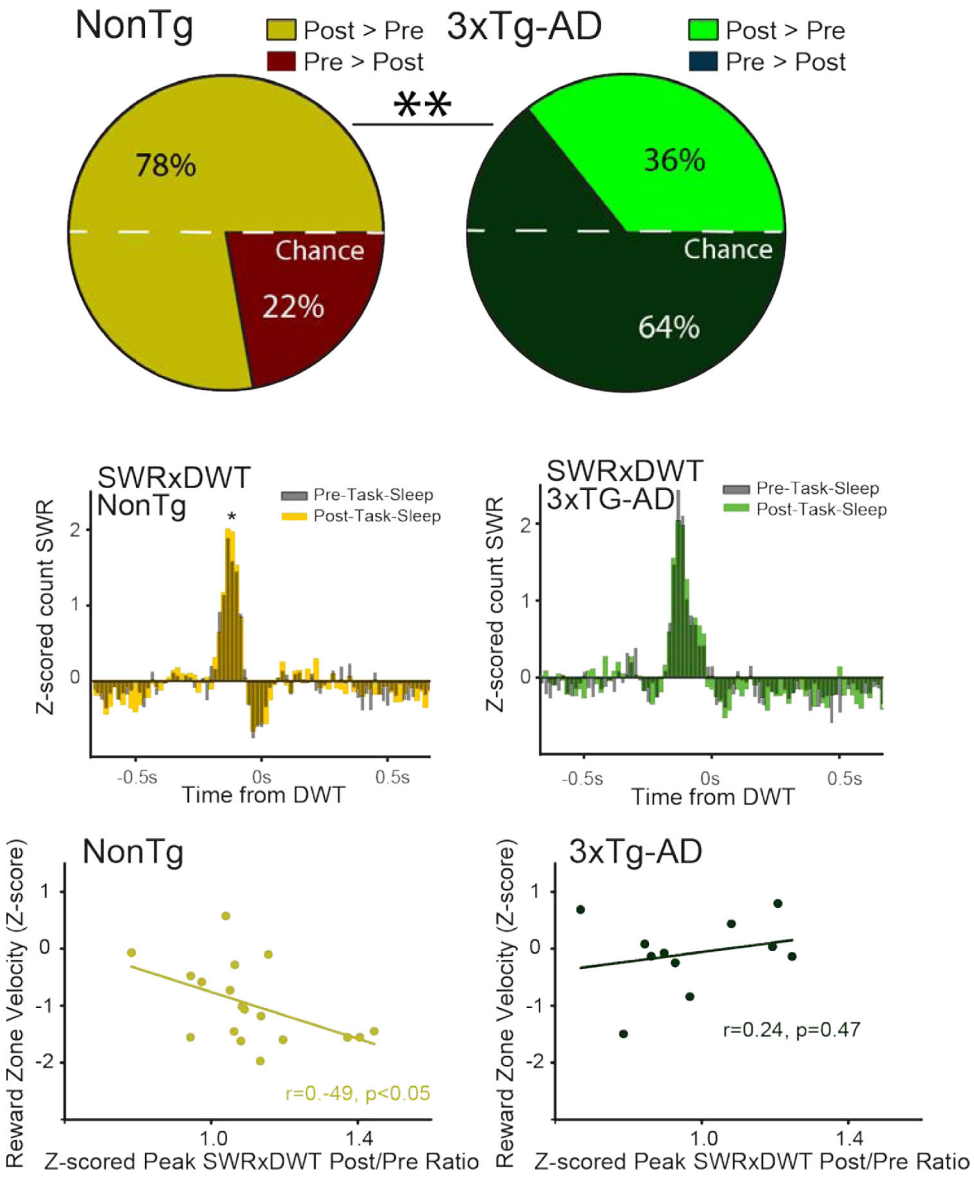

Figure 5. Parietal-hippocampal network coordination is impaired in 3xTg-AD mice and dissociated from behavior.

Top. The proportion of data sets in which the cross-correlation peak was larger in *post-task-sleep* for all NonTg mouse data sets (cream/crimson) and all 3xTg-AD mouse data sets (light/dark green) from the first 6 days of VM training/testing. Hippocampal-PC reactivation event coupling was reduced in 3xTg-AD mice for *post-task-* relative to *pre-task-* sleep. *Middle Left*. Mean Z-scored SWR-DWT cross-correlation for NonTg data sets. SWRs tend to occur in close temporal proximity to DWTs, and this relationship is strengthened in *post-task-sleep* (cream) versus *pre-task-sleep* (black; *p<0.05). *Middle Right*. In 3xTg-AD mice, SWRs occur near DWTs; however, the SWR-DWT correlation is not strengthened in *post-task-sleep* (green) versus *pre-task-sleep* (grey). *Bottom*. Strengthening of DWT-SWR coupling (Z-scored peak SWRxDWT post/pre ratio) is associated with better behavioral

performance the following day (slowing behavior in reward zone) for NonTg (*Left*) but not 3xTg-AD mice (*Right*). See also Figure S1, S5 and Table S2.

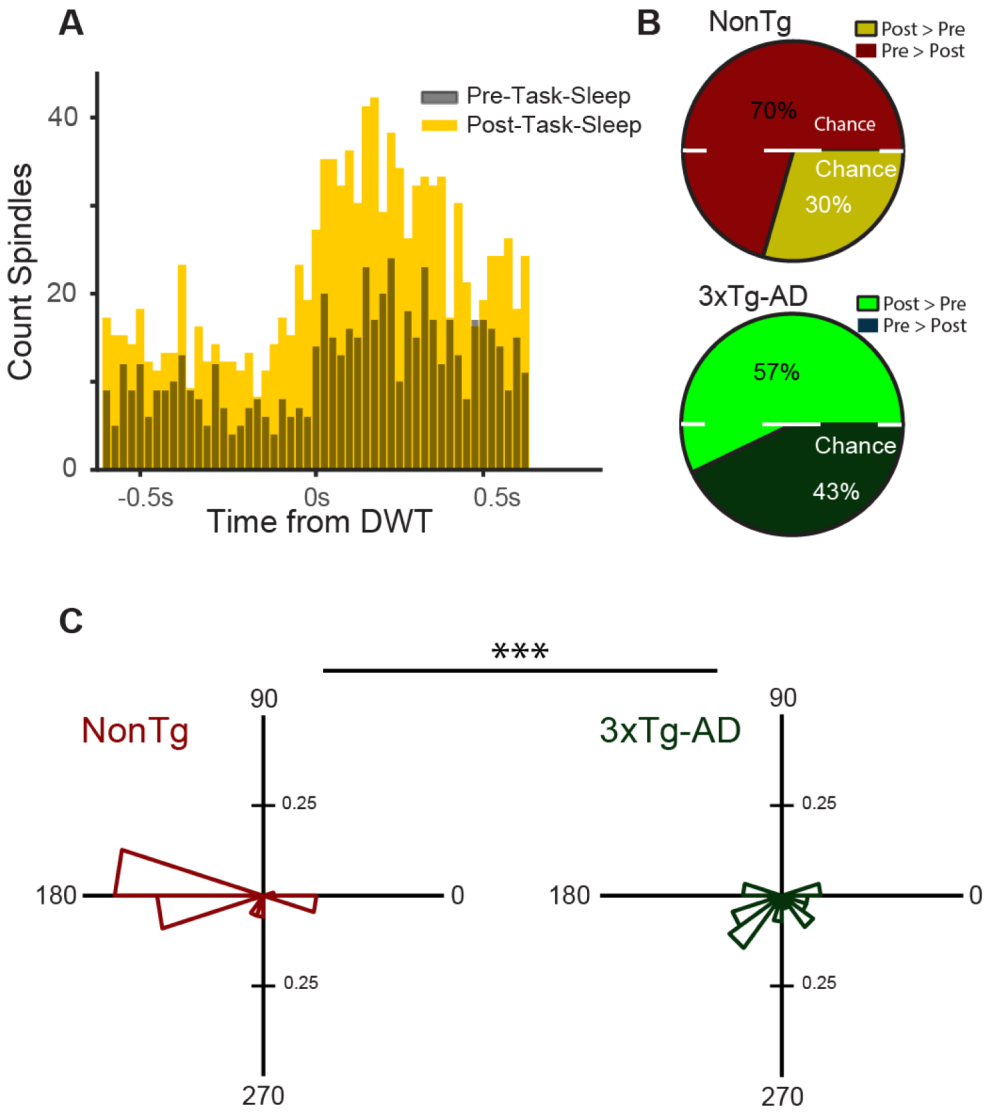

Figure 6. Spindle-DWT coupling is impaired in 3xTg-AD mice.

A. Example spindle-DWT cross-correlation from a NonTg mouse illustrating that for some data sets spindle-DWT coupling is strengthened in *post-task-sleep*. Spindles tend to follow the DWT. **B**. The proportion of data sets in which the cross-correlation peak was not significantly larger in *post-task-sleep* for NonTg (cream/crimson) compared to 3xTg-AD (light/dark green) mouse data sets (p=0.44). **C**. Peak spindle power tends to occur at the peak of the delta wave in NonTg mice (*Left*) but is distributed across delta wave phase in 3xTg-AD mice (*Right*), so the phase distribution is significantly different across genotype. ***p=0.0005. See also Figure S1, S6 and Table S2.

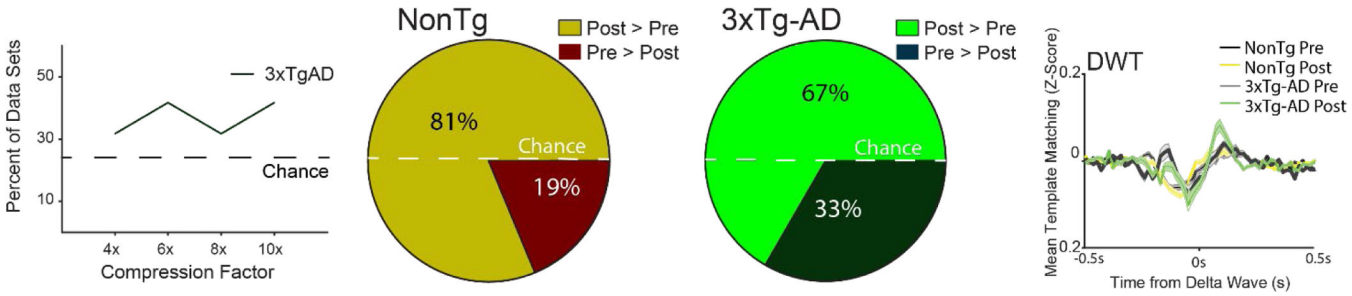

Figure 7. Modest changes in template matching in the PC of 3xTg-AD mice.

Left. The percent of data sets for which template matches are greater in *post-task-sleep* and also greater than non-compressed data for 3xTg-AD mice indicates template matches oscillates around 40% for all compression factors. *Middle*. The proportion of data sets in which there was a higher density of template matches in *post-task-sleep* for NonTg (cream/crimson) and 3xTg-AD (light/dark green) mouse data sets. In PC there was not a significant reduction in template matching in 3xTg-AD mice (p=0.15). *Right*. Event-triggered average template matching Z-score (Mean±SEM) centered on the DWT for *post-task-sleep* for NonTg (cream) and 3xTg-AD (green) mice, relative to *pre-task-sleep* (black-NonTg/grey-3xTg-AD). See also Figure S7 and Tables S1 and S2.

KEY RESOURCES TABLE

REAGENT or RESOURCE	SOURCE	IDENTIFIER
Antibodies		
Anti-β-amyloid 1–16	Biolegend	RRID: AB_2565328
Anti-NeuN	Millipore	RRID: AB_10807945
Anti-mouse-alexa-488	Abcam	RRID: AB_2576208
Anti-rabbit-alexa-594	Invitrogen	RRID: AB_2534095
Anti-NeuN-Cy3	Millipore	RRID: AB_11204707
Anti-phosphorylated-tau	Thermo Scientific	RRID: AB_223647
Anti-mOC78	Abcam	ab205341
Biotinylated goat anti-mouse antibody	Sigma Aldrich	RRID: AB_258604
Anti-parvalbumin	Sigma Aldrich	RRID: AB_477329
Anti-mOC22	Abcam	ab205339
Chemicals, Peptides, and Recombinant Proteins		
Goat serum	Sigma Aldrich	G9023
Triton-X	Sigma Aldrich	X100
Formic acid	Sigma	F0507
Experimental Models: Organisms/Strains		
Mouse: 3xTg-AD: B6;129-Tg(APPSwe,tauP301L)1Lfa *Psen1*^{tm1Mpm}	LaFerla Lab, Bred in-house	n/a
Software and Algorithms		
MATLAB (version 2014b, 2016a)	Mathworks	RRID: SCR_001622
Freely Moving Animal Toolbox (FMAT)	http://fmatoolbox.sourceforge.net/	RRID: SCR_015533
FieldTrip Toolbox	http://www.fieldtriptoolbox.org/	RRID: SCR_004849
Circular Statistics Toolbox	https://es.mathworks.com/matlabcentral/fileexchange/10676-circular-statistics-toolbox-directional-statistics	RRID:SCR_016651
Klustakwik	http://klusta-team.github.io/klustakwik/	RRID:SCR_014480
Mclust	http://redishlab.neuroscience.umn.edu/mclust/MClust.html	n/a
Tablet-VR setup	Leo Molina (leonardomt@gmail.com)	https://github.com/leomol/tablet-vr
StatView	https://www.liebertpub.com/doi/pdf/10.1089/15279160150518540	RRID:SCR_017411
SigmaPlot	http://www.sigmaplot.com/products/sigmaplot/	RRID:SCR_003210
Other		
Digital Lynx 16SX Recording System	Neuralynx	https://neuralynx.com/